AALBORG UNIVERSITET

On Multipath Delay Estimation for OFDM Channel Estimation using Beamforming Techniques

by

Silvio Desiderio

September 2010

"Whatever you do in life will be insignificant
but it is very important that you do it
because nobody else will."

Mahatma Gandhi

AALBORG UNIVERSITET

Abstract

Department of Electronic Systems

by Silvio Desiderio

This thesis investigates estimation of multipath delay components for OFDM-based communication systems. The state-of-the-art channel estimation algorithm for pilot-aided OFDM systems is the Robust Wiener Filter (RWF). An alternative channel estimation method, the Enhanced Noise Reduction Algorithm (ENRA) is also introduced. To analyze and investigate the problem a discrete time OFDM model is derived. We demonstrate by means of simulations how the ENRA outperforms the RWF, with respect to BER, when assuming perfect knowledge of the delay parameters. In order to estimate the delays, the beamforming techniques have been studied. In particular an iterative algorithm, the Sequential Beamforming Algorithm (SBA), is analyzed in this work. Initially it is evaluated for different resolution in the delay domain pointing out how the sequential beamforming performance improves with increasing resolution. Furthermore, it is shown how the performance improves overestimating the number of channels echoes to collect. In the end, we demonstrate by simulations how the ENRA using the SBA as multipath delays estimation tool, outperforms the state-of-the-art algorithm.

Acknowledgements

First of all I would like to show my gratitude to Bernard Fleury and Ernestina Cianca for made this thesis possible and allowing me to have this wonderful experience. I am heartily thankful to my supevisors, Morten L. Jakobsen and Niels L. Pedersen for their help and support during these last six months. Thanks to all the NavCom section for their warm welcome and to all my friends. Finally, I owe my deepest gratitude to my family for the financial and moral support.

Silvio Desiderio
Aalborg, September 2010

Contents

Abstract iv

Acknowledgements v

List of Figures ix

List of Tables xi

Abbreviations xiii

1 Introduction 1
- 1.1 Long Term Evolution . . . 1
- 1.2 Orthogonal Frequency Division Multiplexing . . . 2
- 1.3 Channel Estimation . . . 3
  - 1.3.1 Problem Statement . . . 3
- 1.4 Report structure . . . 5

2 Orthogonal Frequency-Division Multiplexing 7
- 2.1 OFDM System Model . . . 8
  - 2.1.1 IFFT/FFT Implementation . . . 10
- 2.2 Channel Definition . . . 13
  - 2.2.1 Time Varying Channel Impulse Response . . . 13
- 2.3 OFDM in Multipath Channel . . . 15
  - 2.3.1 The Cyclic Prefix . . . 16
  - 2.3.2 Matrix Representation . . . 17
- 2.4 OFDM Summary . . . 19

3 State-of-the-art summary 21
- 3.1 Channel Estimation . . . 21
  - 3.1.1 Pilot Symbol Observation . . . 22
  - 3.1.2 Enhanced Noise Reduction Algorithm . . . 22
  - 3.1.3 Robust Wiener Filter . . . 23
- 3.2 Performance Comparison . . . 24

4 Beamforming 27
- 4.1 Framework and assumptions . . . 27

4.2 Conventional Beamformer 29
4.3 Capon Beamformer 31
4.4 SBA 32
4.5 SBA Features 34
4.6 Beamforming Summary 36

5 Simulations and Results **37**
5.1 Simulation setup 37
5.2 Grid Search Sampling 39
5.2.1 Parabola approximation 41
5.2.2 Left/right search 42
5.3 The Number Of Delays 44
5.4 Chapter Summary 44

6 Conclusions and Future Work **47**
6.1 Future Work 47

A LTE System Setup **49**
A.1 Unused subchannels 49
A.2 Radio frame structure 50
A.3 Pilot position 51

Bibliography **55**

List of Figures

1.1 Subcarriers and OFDM symbol . . . 3
1.2 Representation of a train of six pulses in a multipath channel . . . 4

2.1 Single Carrier and Multiple Carrier Modulation . . . 8
2.2 Digital OFDM System . . . 11
2.3 Multipath scenario with LoS component (solid line) and two reflected components (dotted lines) . . . 13
2.4 Cyclic prefix and ISI . . . 16

3.1 Performance of the ENRA with true delays compared with RWF . . . 25

4.1 A beamformer output . . . 29
4.2 Conventional Beamforming . . . 31
4.3 Normalized Capon's spectrum, 10 dB SNR, 200 snap-shots . . . 32
4.4 SBA iteration . . . 34
4.5 Sinc function normalized to the maximum value . . . 35
4.6 Dominant contribution to the beamforming output . . . 36

5.1 Pilot symbols pattern for simulator . . . 39
5.2 Structure of the used simulator . . . 40
5.3 BER for different value of grid resolution . . . 41
5.4 MSE for different value of grid resolution . . . 41
5.5 Parabola approximation . . . 42
5.6 BER for parabola approximation . . . 42
5.7 The left/right search method . . . 43
5.8 BER/SNR with left/right approximation . . . 43
5.9 BER with overestimated number of delays . . . 44

A.1 Placement of the subcarriers in LTE setup . . . 49
A.2 Radio frame structure . . . 51
A.3 Pilot pattern SISO . . . 52
A.4 Pilot pattern MIMO . . . 53

List of Tables

1.1 LTE system attributes 2

5.1 Extended Vehicular A model (by 3GPP) 38
5.2 Extended Vehicular A profile shifted 10 sample to right of zero 38
5.3 Accuracy and number of iteration 43

A.1 LTE parameters 50

Abbreviations

LTE	**L**ong **T**erm **E**volution
GSM	**G**lobal **S**ystems for **M**obile communications
UMTS	**U**niversal **M**obile **T**elecommunications **S**ystem
3GPP	**3**rd **G**eneration **P**artnership **P**roject
OFDM	**O**rthogonal **F**requency **D**ivision **M**ultiplexing
ISI	**I**nter **S**ymbol **I**nterference
ICI	**I**nter **C**arrier **I**nterference
QAM	**Q**uadrature **A**mplitude **M**odulation
PSK	**P**hase **S**hift **K**eying
DFT	**D**iscrete **F**ourier **T**ransform
IDFT	**I**nverse **D**iscrete **F**ourier **T**ransform
FFT	**F**ast **F**ourier **T**ransform
IFFT	**I**nverse **F**ast **F**ourier **T**ransform
PACE	**P**ilot **A**ssisted **C**hannel **E**stimation
RWF	**R**obust **W**iener **F**ilter
ENRA	**E**nhanced **N**oise **R**eduction **A**lgorithm
SBA	**S**equential **B**eamforming **A**lgorithm
SNR	**S**ignal to **N**oise **R**atio
BER	**B**it **E**rror **R**ate
EPA	**E**xtended **P**edestrian **A**
EVA	**E**xtended **V**ehicular **A**
ETU	**E**xtended **T**ypical **U**rban
GMSK	**G**aussian **M**inimum **S**hift **K**ey
TDMA	**T**ime **D**ivision **M**ultiple **A**ccess
CDMA	**C**ode **D**ivision **M**ultiple **A**ccess

MIMO	**M**ultiple **I**nput **M**ultiple **O**utput
ESPRIT	**E**stimation of **S**ignal **P**arameters by **R**rotational **I**nvariance **T**echniques
AWGN	**A**dditive **W**hite **G**aussian **N**oise
ADSL	**A**symmetric **D**igital **S**ubscriber **L**ine
DAB	**D**igital **A**udio **B**roadcasting
DAB	**D**igital **V**ideo **B**roadcasting
LoS	**L**ine of Sight

To my Family...

Chapter 1

Introduction

This report has been inspired by the previous work by Morten Lomholt Jackobsen [1] and Kim Laugesen [2] and it aspires to be a continuation. In particular we investigate a tap-delay detection algorithm for channel estimation in an OFDM receiver. OFDM is the multicarrier modulation adopted in the 3GPP standard for downlink LTE. The report has been written thinking to this OFDM application but without strictly follow the LTE standard technical specifications.

In this chapter some background information are presented in order to understand the problem concerning the channel estimation task. In Section 1.1 we provide information concerning the LTE standard and in Section 1.2 the basic idea of OFDM is presented. In order to provide a general overview of channel estimation, we discuss the state-of-the-art in Section 1.3.

1.1 Long Term Evolution

The evolution of wireless communication systems and networks in recent years has been explosive and the interest concerning this field has led a real revolution in terms of speed, reliability and quality of service. Especially in the mobile communications field always more service are available in the last generation of cell phone. Cellular system is now the dominant two-way mobile communications technology. The first generation of cellular systems, introduced in 1980, was voice-only and it used analog communications. Second generation systems moved from analog to digital because of the latter's many advantages [3]. The modulation used in GSM is the *Gaussian Minimum Shift Key* (GMSK) with *Time Division Multiple Access* (TDMA) used in order to provide a multiple channel access. Then, the third generation cellular system is the *Universal*

Mobile Telecommunications System (UMTS) where the bigger innovation is the access that employs the *Code Division Multiple Access* (CDMA). LTE is an evolution of the current 3G standards introduced in order to provide a long term standardization that can be used by the mobile communication industry for the next decade and longer. It is collocated between 3G standards, like UMTS, and the 4th generation standards still under development. The goal of LTE is to provide a high-data-rate, low latency and packet-optimized radio-access technology supporting flexible bandwidth deployments [4]. The system supports flexible bandwidths thanks to OFDM architecture. It is optimized for low speeds up 15 Km/h, however the specifications allow mobility support in excess of 350 Km/h with some performance degradation [5]. The downlink is implemented in a 4×4 *Multiple Input Multiple Output* (MIMO) system within 20 MHz bandwidth and with peak data rates of 326 Mb/s. In the uplink MIMO is not employed in the first release of the LTE standard and the data rates is lower than 86 Mb/s. In Table 1.1 are summarized some LTE system attributes [5].

Bandwidth	$1.25 - 20$ MHz
Mobility	350 Km/h
MIMO Downlink	2×2, 2×4, 4×4
MIMO Uplink	1×2, 1×4
Modulation	QPSK, 16-QAM and 64-QAM
Channel coding	Turbo code

TABLE 1.1: LTE system attributes

1.2 Orthogonal Frequency Division Multiplexing

The current 3G systems use a *Wideband Code Division Multiple Access* (WCDMA) scheme with 5 MHz bandwidth in both downlink and uplink [5]. In order to satisfy the aggressive LTE requirements, it is needed to employ a new access scheme in the LTE downlink. OFDM is the approach proposed by 3GPP in the LTE standards. The basic idea of OFDM is to divide the entire spectrum into a defined number of narrowband channels that are supposed to be not selective in time and frequency. The overall data rate is split into several lower data rates, each one corresponding to a different subcarrier. Then, the purpose of this approach is to let each channel experience almost flat-fading response in order to simplify the channel equalization process. Furthermore, due to the orthogonality between the subcarriers is possible to allow a subchannels overlap increasing the spectral efficiency. In Figure 1.1 is shown an example of five subchannels or subcarriers at different frequencies. When the signal pass through a time-dispersive radio channel, the inter-OFDM symbol interference could cause lost of orthogonality between OFDM subcarriers. However a cyclic prefix is used in order to avoid this

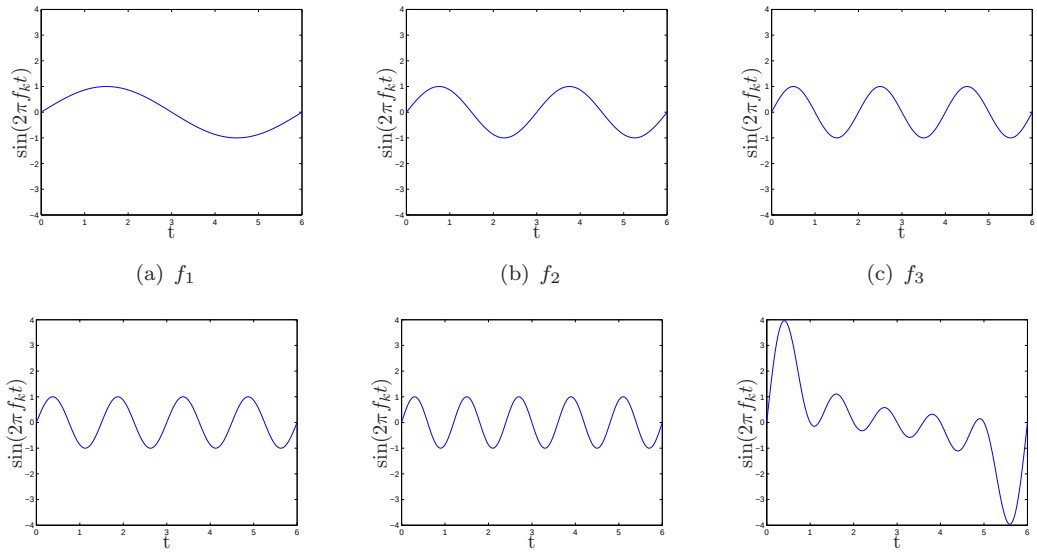

(a) f_1 (b) f_2 (c) f_3

(d) f_4 (e) f_5 (f) OFDM symbol

FIGURE 1.1: An example of five OFDM subcarriers at frequencies f_1, f_2, f_3, f_4, f_5 all modulated with the same symbol. In figure (f) is shown the OFDM symbol. It is formed adding the modulated subcarrier signals

interference. The cyclic prefix length is choose longer than the maximum delay spread. The process of modulating the information symbols into different subchannels is carried out by use of *Discrete-time Fourier Transform* (DFT). It is implemented, with low complexity and high efficiency, through the *Fast Fourier Transform* (FFT).

1.3 Channel Estimation

As earlier mentioned the transmission scenario is a time-dispersive radio channel that, as known, suffers the multipath effects. The signal interacts with many object in the environment creating multiple copies of the transmitted signal attenuated, shifted in phase and delayed in time. In the most general case, the channel parameters are not fixed during the transmission time. However, in order to simplify our model a static approximation is assumed.

1.3.1 Problem Statement

If a single narrowband pulse is transmitted on a multipath channel, the received signal is a pulse train where each pulse corresponds to a different path. In Figure 1.2 is illustrated a delay axis with six echoes received. Each arrow represents a single signal copy that is attenuated and delayed; τ_l with $l = 1, \ldots, 6$ is the delay associated to the l-th path. In the general case the delays of the multipath channel and the number of delays, change

over time due to the mobility of the user and/or the object in the environment. For simplicity, throughout this work, we assume it fixed during the transmission of each OFDM symbol.

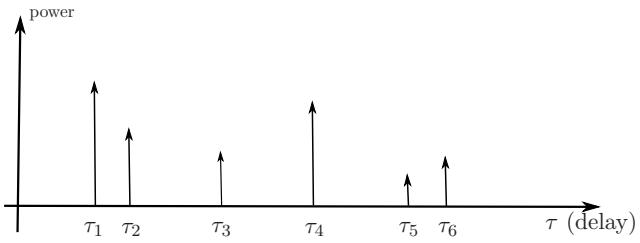

FIGURE 1.2: Representation of a train of six pulses in a multipath channel

In order to carry out the channel estimation, assuming the above model, it is really important to estimate the correct position of the delays. In [6–8] several techniques for channel estimation in OFDM system are suggested. These methods are all based on the *Pilot Assisted Channel Estimation* (PACE) approach in two dimensions (time and frequency domain). The basic principle of PACE algorithms is to transmit symbols known to the receiver into the data stream and spread in time and frequency domains. Hence, the receiver is able to perform the estimation at any time given the observation at the pilot locations. The existing state-of-the-art algorithm, the Robust Wiener Filter, does not need the knowledge of the delay positions but it suffers from an irreversible form of degradation due to the robust setup. In [1] is suggested to use an alternative channel estimator, the *Enhanced Noise Reduction Algorithm* (ENRA). The ENRA is based on a particular observation model that we study in Chapter 3. In particular it use some critical assumptions: the number L of channel component and the the delay parameters are assumed to be known. Under these assumptions the ENRA is able to outperform the state-of-the-art algorithm. However, if the delays are not perfectly known, and they are not in practice, there is a performance degradation especially for high value of SNR. In order to estimate correctly the delay parameters some algorithms have been suggested in [1, 2]: *Estimation of Signal Parameters by Rotational Invariance Techniques* (ESPRIT) and *Sequantial Beamforming Algorithm* (SBA). The attention is focused on the latter that is investigated in Chapter 4. Different beamforming approach are presented: Conventional Beamformer, Capon Beamformer and Sequential Beamformer. Major attention is given to the latter because it is a good compromise between performance and complexity. This algorithm is proposed in [9] for automatic signal source localization in passive sensor arrays. It has been adapted to our tap-delay estimation problem allowing interesting simulation-based comparisons. In particular, in terms of BER, we compare the state-of-the-art algorithm with the ENRA using sequential beamforming as multipath delays estimation tool.

1.4 Report structure

The thesis is divided into six chapters, where the first chapter is the introduction that include background information about LTE, OFDM and state-of-the-art algorithm for channel estimation. In Chapter 2, 3, 4 the background theory to OFDM and channel estimation is presented. In Chapter 5 the simulation setup and the results are shown. Chapter 6 contains conclusions and motivations for future work.

Chapter 2

Orthogonal Frequency-Division Multiplexing

Orthogonal Frequency Division Multiplexing is a multicarrier technique in which the basic idea is to split the entire system bandwidth, into a defined number N of narrowband channels which are supposed to be non-selective in time and frequency. The informative flow incoming at the modulator is divided and afterward transmitted on each channel with a lower bit rate. The most important implication is the reduction of the *Inter-Symbol Interference* (ISI) due to the lower bandwidth occupation of each subchannel. Unlike the classical *Frequency Division Multiplexing* (FDM), the subcarriers are chosen orthogonal providing a high spectral efficiency. OFDM is very flexible in the usage of bandwidth and is particularly suitable for multipath environments. For these reasons it is found in many applications in the following fields:

- Wideband wireless network: standard IEEE 802.11 and IEEE 802.16 (WiMax)
- Broadcasting service: DAB (*Digital Audio Broadcasting*), DVB(*Digital Video Broadcasting*)
- Cabled network: ADSL (*Asymmetric Digital Subscriber Line*)

OFDM for LTE downlink transmission scheme is studied in this chapter. The working principles and the IFFT/FFT OFDM implementation will be introduced in the first part. An useful matrix representation of the signal model is shown in the Section 2.3.2.

2.1 OFDM System Model

A multipath channel is characterized by a time variant transfer function $h(f,t)$ due to fading and user terminal mobility. Ideally, we would have a flat response in both the frequency domain and the time domain. This means that the system bandwidth B should be lower than the coherence bandwidth (frequencies interval in which the channel amplitude response is constant) and the coherence time (interval in which the channel can be considered time invariant) is bigger than the symbol time $\tau_s = 1/B$. This condition may be not satisfied when the system bandwidth is big. Therefore, if we use single carrier modulation it may be complicated to carry out the channel equalization and channel estimation is frequently required. The principal idea of OFDM is to divide the entire bandwidth obtaining N narrowband channels not frequency selective (Figure 2.1) and symbols with longer duration. The symbols transmitted on each subchannel

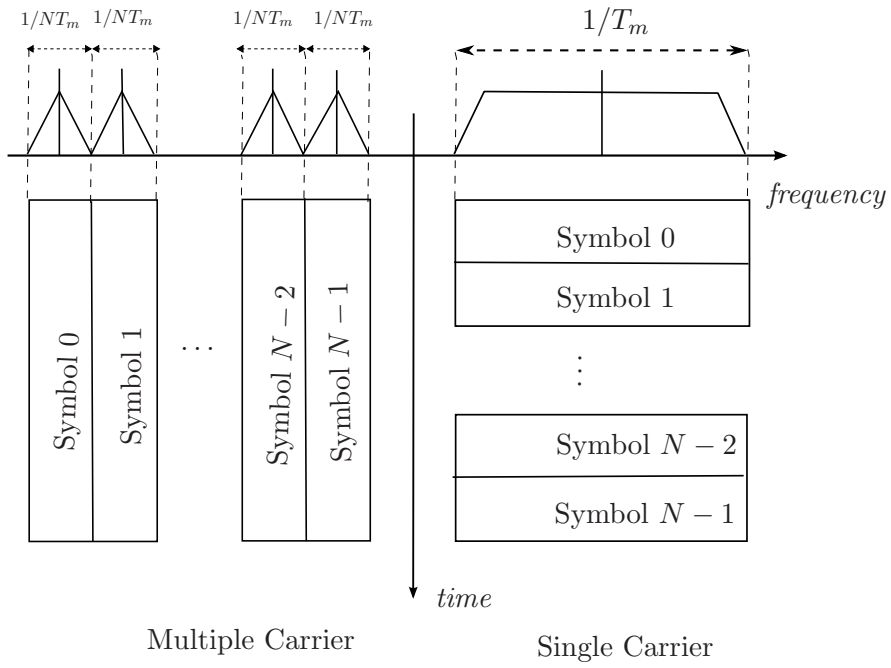

FIGURE 2.1: Distinction between Single Carrier and Multiple Carrier Modulation

are N times longer than the symbols transmitted in single carrier modulation. With the symbol duration prolonged, ISI is small and it can be completely eliminated by the insertion of cyclic prefix (discussed in Section 2.3.1). QAM or PSK modulation is usually employed for OFDM transmission in selective and time-variant channels. For simplicity, throughout this work we consider QPSK modulation where four bits are associated to each symbol. Therefore the informative flow incoming at the OFDM modulator is divided into blocks of size $N \times 4$. Afterwards each block is associated with an OFDM symbol, serial to parallel converted and transmitted on one of the N

orthogonal subcarriers available. The OFDM symbol duration is $T_s = N\tau_s$ and the occupied bandwidth become smaller than the channel coherence bandwidth. By choosing a large enough N, it is possible to transmit with a high bit rate, with low symbol rate on each subcarrier and hence reducing ISI. The baseband signal within an OFDM symbol read as [5]

$$s(t) = \sum_{k=0}^{N-1} X(k) e^{j2\pi k\Delta f t} \tag{2.1}$$

where N is the number of subcarriers, $\Delta f = 1/T_s$ is the subcarriers spacing and $X(k)$ is the complex modulation symbol transmitted on the k-th subcarrier. The signal incoming at the receiver side is multiplied with $e^{-j2\pi m\Delta f t}$ and integrated over an OFDM symbol duration. Then the estimate of the complex modulation symbol $X(m)$ is given by

$$\widehat{X}(m) = \frac{1}{T_s} \int_0^{T_s} [s(t) + n(t)]\, e^{-j2\pi m\Delta f t} dt \tag{2.2}$$

Assuming perfect synchronization in both time and frequency domain and ignoring the time and frequency dispersion due to the wireless channel, the transmitted data signal is perfectly recovered and the only degradation is the *Additive White Gaussian Noise* (AWGN) component, $n(t)$. By letting

$$\widetilde{n} = \frac{1}{T_s} \int_0^{T_s} n(t) e^{-j2\pi m\Delta f t} dt$$

the equation (2.2) can be written as

$$\widehat{X}(m) = \frac{1}{T_s} \sum_{k=0}^{N-1} X(k) \int_0^{T_s} e^{j2\pi(k-m)\Delta f t} dt + \widetilde{n} = X(m) + \widetilde{n}$$

Then, under the above assumptions of perfect time and frequency synchronization and ignoring the effect of wireless channel, the transmitted signal is perfectly recovered with the only degradation due to the noise. This is guaranteed by the orthogonality between OFDM subcarriers over the symbol duration T_s. Consider a set of functions $\{\varphi_{i,k}(t)\}$ where i is the OFDM symbol index [3]

$$\varphi_{i,k}(t) = \begin{cases} e^{j2\pi k\Delta f t} & iT_s < t < (i+1)T_s \\ 0 & otherwise \end{cases}$$

It is possible to verify that $\varphi_{i,k}(t)$ is a set of orthogonal function, that is:

$$\int_{-\infty}^{+\infty} \varphi_{i,k}(t)\varphi^*_{i',k'}(t) dt = \begin{cases} T_s & when \quad i = i' \quad \text{and} \quad k = k' \\ 0 & \text{otherwise} \end{cases}$$

For $i \neq i'$ the functions temporal range are disconnected and the integral is equal to zero. Indeed supposing $i = i'$ the integral is equal to:

$$\int_{iT_s}^{(i+1)T_s} e^{j2\pi k\Delta f t} e^{-j2\pi k\Delta f t} dt = \int_{iT_s}^{(i+1)T_s} e^{j2\pi(k-k')\Delta f t} dt$$

- if $k \neq k'$ we are considering two different carriers and the integral in the above equation is equal to zero.
- if $k = k'$ we are considering the same carrier:

$$\int_{-\infty}^{+\infty} \varphi_{i,k}(t)\varphi^*_{i',k'}(t)dt = \int_{iT_s}^{(i+1)T_S} |\varphi_{i,k}(t)|^2 dt = T_s$$

Carriers orthogonality is an underlying aspect of OFDM systems because it allow to reconstruct the received symbol even if the subchannels are overlapped in the frequency domain.

2.1.1 IFFT/FFT Implementation

It's evident that for big value of N, the analogue modulation is not achievable due to the huge number of oscillators required. In what follows, we derive a digital implementation of the OFDM signal based on the *Discrete Fourier Transform* (DFT) and its fast implementation FFT (*Fast Fourier Transform*). For this purpose, we consider the OFDM signal complex envelope [5]:

$$\widetilde{s}(t) = \sum_{i=-\infty}^{+\infty} \sum_{k=0}^{N-1} X_i(k)\ e^{j2\pi k\Delta f t}\ rect(\frac{t}{T_s} - i) \tag{2.3}$$

where *rect* is a window function defined as

$$rect(t) = \begin{cases} 1 & \forall t \in (0, 1] \\ 0 & \text{elsewhere} \end{cases}$$

Recalling the equation (2.1), the signal complex envelope of a generic OFDM symbol i.e. not considering the index i in (2.3), is given by

$$s(t) = \sum_{k=0}^{N-1} X(k)\ e^{j2\pi k\Delta f t} \qquad t \in (iT_s, (i+1)T_s] \tag{2.4}$$

Sampling, N times, the OFDM symbol at time instants $t = \frac{m}{N}T_s$ the above equation can be written as

$$s(\frac{m}{N}T_s) = \sum_{k=0}^{N-1} X(k)\ e^{j2\pi k\frac{m}{N}} \qquad m = 0, 1, 2, \ldots, N-1 \tag{2.5}$$

We can represent $s(\frac{m}{N}T_s)$ as $s(m)$ as it depends upon m. Then the above equation can be written as

$$s(m) = N\ IDFT\left\{X(k)\right\} \qquad k, m = 0, 1, 2, \ldots, N-1$$

where

$$IDFT\left\{X(k)\right\} = \frac{1}{N}\sum_{k=0}^{N-1} X(k)\ e^{j2\pi k\frac{m}{N}}$$

is the *Inverse Discrete Fourier Transform* (IDFT) of the samples $X(k)$ [3]. The IDFT is typically implemented via hardware through the more efficients FFT and *Inverse FFT* (IFFT) algorithms. Then, the complex modulation symbols $X(k)$ $k = 0, 1, 2, \ldots, N-1$ are mapped to the input of IFFT. Considering these observations a digital implementation of baseband OFDM transmitter/receiver is shown in Figure 2.2.

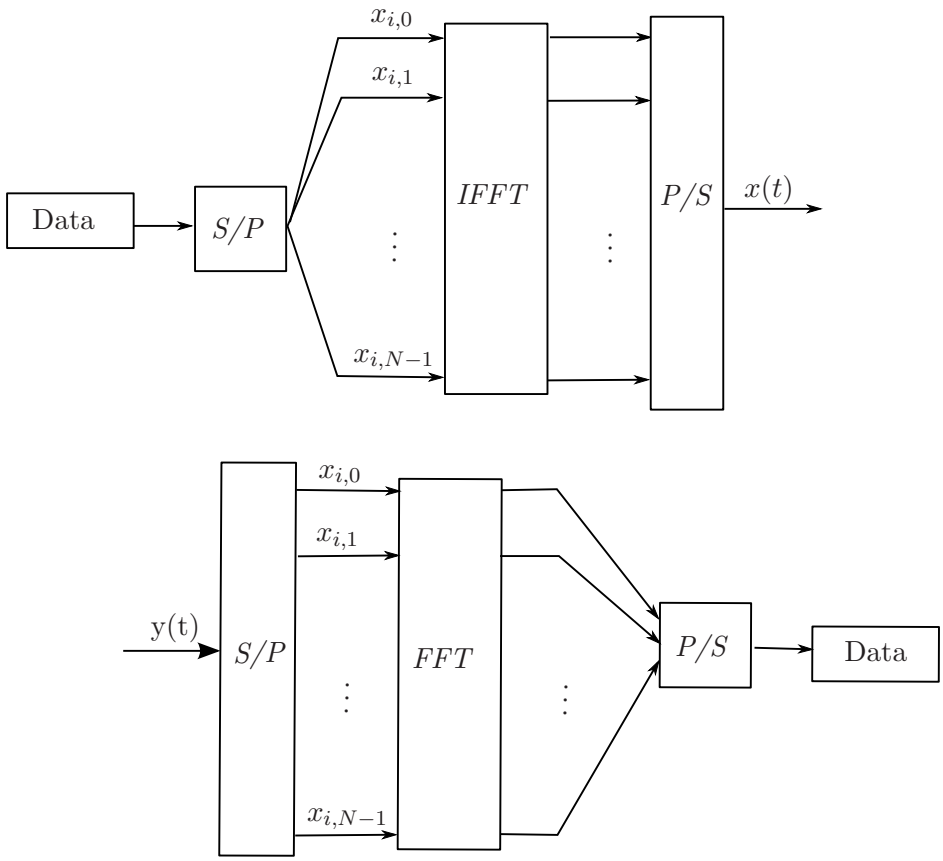

FIGURE 2.2: Digital OFDM System

Even for the demodulator we can easily get an OFDM implementation by inverting (2.5):

$$X(k) = \sum_{m=0}^{N-1} s(m) e^{-j2\pi \frac{km}{N}} \Rightarrow NX(k) = DFT(x(m)) \tag{2.6}$$

The N-point DFT on the complex envelope samples provides the elementary symbol modulating the N carrier. In the forthcoming chapters let $\widetilde{\boldsymbol{x}} = [\widetilde{x}_1, \widetilde{x}_2, \ldots, \widetilde{x}_N]^T$ be the $N \times 1$ column vector of PSK (or QAM) modulated symbols and $\boldsymbol{x} = [x_1, x_2, \ldots, x_N]^T$ the vector after the IDFT. So the N-point DFT of $\boldsymbol{x}$ produce the column vector $\widetilde{\boldsymbol{x}}$. Introducing the $N \times N$ Fourier matrix

$$F = \frac{1}{\sqrt{N}} \begin{bmatrix} 1 & 1 & 1 & \ldots & 1 \\ 1 & \omega & \omega^2 & \ldots & \omega^{N-1} \\ 1 & \omega^2 & \omega^4 & \ldots & \omega^{2(N-1)} \\ \vdots & \vdots & \vdots & \ddots & \vdots \\ 1 & \omega^{N-1} & \omega^{2(N-1)} & \ldots & \omega^{(N-1)^2} \end{bmatrix} \tag{2.7}$$

where $\omega := e^{-j2\pi \frac{1}{N}}$, we can recast the N-point DFT as:

$$\widetilde{\boldsymbol{x}} = F\boldsymbol{x} \tag{2.8}$$

Matrix F is unitary, so we can write the following identity:

$$FF^H = F^H F = I \tag{2.9}$$

Indicating with $F(l, m)$ the entry in row l and in column m of F:

$$F(l, m) = \frac{1}{\sqrt{N}} \omega^{(l-1)(m-1)}, \qquad l, m \in \{1, 2, \ldots, N\}$$

the product (2.9) can be written as:

$$\begin{aligned} FF^H(l, m) &= \sum_{i=1}^{N} F(l, i) F^*(i, m) = \frac{1}{N} \sum_{i=1}^{N} \omega^{(l-1)(i-1)} \omega^{-(i-1)(m-1)} \\ &= \frac{1}{N} \sum_{i=1}^{N} \omega^{(i-1)(l-m)} = \begin{cases} 1 & \text{if} \quad m = l \\ 0 & \text{if} \quad m \neq l \end{cases} \end{aligned} \tag{2.10}$$

where for $m \neq l$ we have a sum of N complex number on the unit circle in the complex plane, that is equal to zero. From (2.10), the product FF^H is equal to the identity matrix, therefore $F^{-1} = F^H$. Therefore the IDFT can be written as:

$$\boldsymbol{x} = F^H \widetilde{\boldsymbol{x}}$$

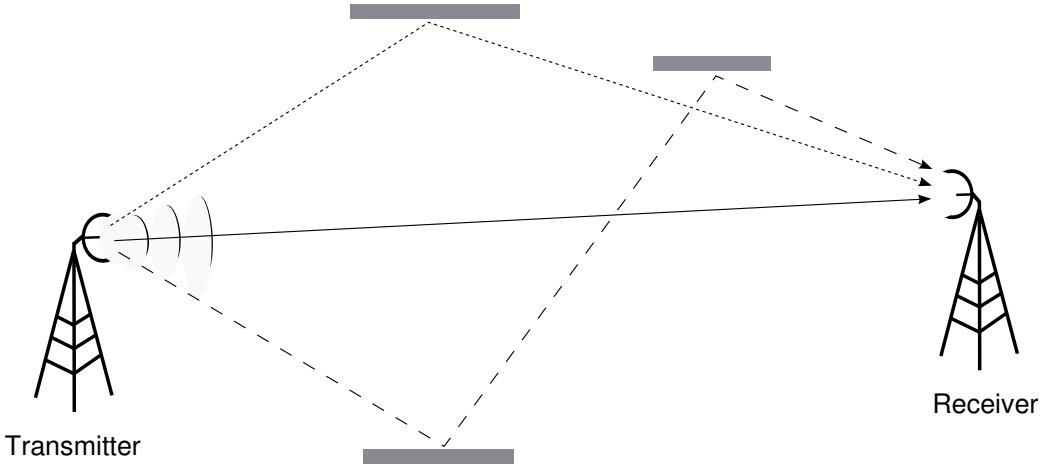

FIGURE 2.3: Multipath scenario with LoS component (solid line) and two reflected components (dotted lines)

2.2 Channel Definition

In this section a channel affected by multipath propagation is examined and the main part is inspired by [3]. Consider a radio signal transmitted from a fixed source as shown in Figure 2.3. The signal interacts with many objects in the environment producing multiple copies of the transmitted signal i.e. mutipath signal components. These multipath signals might be attenuated in power, shifted in phase and/or frequency and delayed in time. For this reason when they are all combined at the receiver side, the reconstructed signal is distorted. Indeed if a single narrow pulse is transmitted the received signal is a pulse train and each component corresponds to a different path. If a direct path exists (unbroken line in Figure 2.3) the first pulse received is the *Line of Sight* (LoS) component, while the last one is associated with the longest path. However, for simplicity we assume a *not Line of Sight* (nLoS) Rayleigh fading channel. Furthermore the multipath channel have a time-varying impulse response if either the transmitter, receiver or the environment are moving.

2.2.1 Time Varying Channel Impulse Response

Let consider the transmitted bandpass signal modeled as [3]

$$s(t) = \Re\left\{x(t)e^{j2\pi f_c t}\right\}$$

where f_c is the carrier frequency, $x(t) = s_I(t) + js_Q(t)$ is called complex envelope or equivalent low-pass signal of $s(t)$; $s_I(t) = \Re\{x(t)\}$ is the in-phase component and $s_Q(t) = \Im\{x(t)\}$ is the quadrature component. The received signal is given by the sum of the

all resolvable multipath components

$$r(t) = \Re\left\{\left(\sum_{l=0}^{L(t)} \alpha_l(t)x(t-\tau_l(t))e^{-jD_l(t)}\right)e^{j2\pi f_c t}\right\} \tag{2.11}$$

where

- $\alpha_l(t)$ is a complex amplitude associated with the l-th delay
- $L(t)$ is the number of multipath components
- $\tau_l(t)$ is the l-th delay
- $e^{-jD_l(t)}$ is the Doppler phase shift for the l-th multipath component.

All the above terms are unknown. In particular all the interactions with the objects in the wireless medium cause a change in the phase term $e^{-jD_l(t)}$. Let consider that only the transmitter is moving, the Doppler shift read as

$$D_l(t) = 2\pi f_c \tau_l(t) = 2\pi \frac{l_l(t)}{\lambda_l} = \frac{2\pi}{\lambda_l}\left(l_0 + v\cos(\theta_l)t\right)$$

where

- $l_l(t)$ is the length of the propagation path relative to the l-th signal component and l_0 the distance between transmitter and receiver before the movement
- v is the speed of the receiver
- θ_l is the angle between the incoming component and the direction of the receiver movement
- λ_l is the carrier wavelength

Furthermore the duration of the received signal in (2.11) depends on the channel delay spread τ_m. Comparing it with the signal length $T = \frac{1}{B_x}$ of the baseband signal $x(t)$

- if $\tau_m >> T$ severe ISI is introduced
- if $\tau_m << T$ negligible ISI is introduced

For what just said it is desirable to have a small τ_m and B_x (then a big T). On the other hand, two delays are resolvable only if

$$|\tau_1 - \tau_2| >> \frac{1}{B_x}$$

Otherwise the received signal component can not be separated and they are added into a single component at the delay $\tau \approx \tau_1 \approx \tau_2$. The received signal in (2.11) can be written as the convolution between the channel impulse response and the transmitted signal $x(t)$.

$$r(t) = \Re\left\{\left[\int_{-\infty}^{+\infty}\sum_{l=0}^{L(t)}\alpha_l(t)e^{-jD_l(t)}\delta(t-\tau_l(t))x(t-\tau)d\tau\right]e^{j2\pi f_c t}\right\}$$

$$= \Re\left\{\left[\int_{-\infty}^{+\infty} g(\tau,t)x(t-\tau)d\tau\right]e^{j2\pi f_c t}\right\}$$

where $\delta(t)$ is the Dirac's delta. The impulse response is given by

$$g(\tau,t) = \sum_{l=0}^{L(t)}\alpha_l(t)e^{-jD_l(t)}\delta\left(t-\tau_l(t)\right)$$

Then the impulse response is time variant because depends on the time t. For simplicity, throughout this work the following time invariant channel is assumed during the transmission of a single OFDM symbol

$$g(\tau) = \sum_{l=0}^{L}\alpha_l\delta\left(\tau-\tau_l\right) \tag{2.12}$$

where the Doppler shift is included in α_l such that:

$$\alpha_l = \alpha_l e^{-j2\pi f_c\tau_l}$$

2.3 OFDM in Multipath Channel

As mentioned shortly in the beginning of this chapter, OFDM provides very good performance in multipath environment especially with regard to ISI minimizing. The transmission of big informative flow requires to use very small symbols time T_s. In selective channel, it is advised against to use high-performance modulations because they are very vulnerable to errors. Consequently, small value of T_s cause a big value of ISI. Using OFDM is possible to increase the symbol time T_s acting on the subcarriers number and consequently minimize ISI. We can not arbitrarily increase the value of N so, for completely eliminate the interference, OFDM uses a time guard inside each symbol.

2.3.1 The Cyclic Prefix

In OFDM, the time guard insertion is realized replying in the head of each symbol a number equal to μ of the last sequence samples (see Figure 2.4). This sequence is called *cyclic prefix* [3]. The number μ is chosen longer than the impulse response of the channel, to avoid interference between two adjacent symbols.

$$\begin{aligned} x_{cp}[0] &= x[N-\mu] \\ x_{cp}[1] &= x[N-\mu+1] \\ &\vdots \\ x_{cp}[\mu] &= x[0] \\ x_{cp}[\mu+1] &= x[1] \\ &\vdots \\ x_{cp}[N+\mu] &= x[N] \end{aligned} \tag{2.13}$$

The use of cyclic prefix causes a loss of spectral efficiency and a waste of energy. About the latter, we could transmit nothing for saving energy, but the absence of transmission during the guard time cause a loss of frequency orthogonality between carrier, introducing *Inter-Carrier Interference* (ICI).

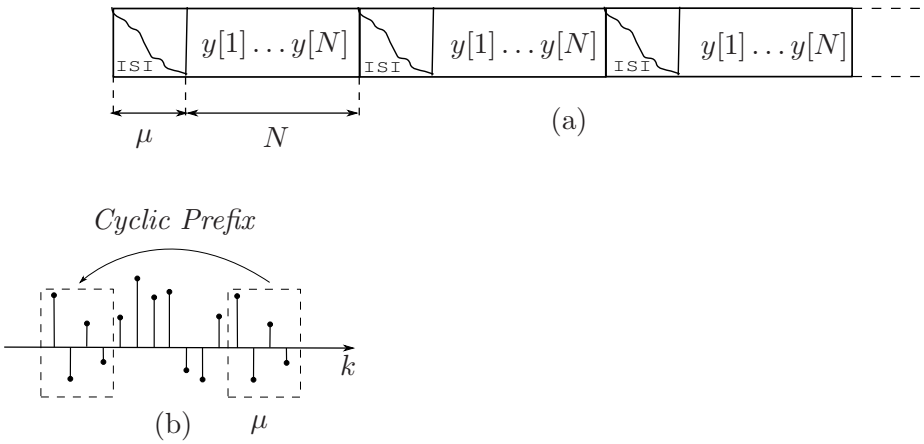

FIGURE 2.4: ISI between data blocks in channel output (a) and cyclic prefix construction (b)

Another effect of the cyclic prefix insertion is that it turns the linear convolution between the $N+\mu$ coefficients of the sampled signal and the channel impulsive response, into a

circular convolution. Considering the DFT of the channel output in absence of noise

$$Y[m] = \text{DFT}\{y(n) = x(n) \otimes h(n)\} = X(m)H(m) \qquad 0 \leq m \leq N-1$$

and the input sequence $x(n)$ can be recovered from the channel output $y(n)$, if we know $h(n)$ by

$$x(n) = \text{IDFT}\left\{\frac{Y(m)}{H(m)}\right\} = \text{IDFT}\left\{\frac{\text{DFT}\{y(n)\}}{\text{DFT}\{h(n)\}}\right\}$$

Thus, the cyclic prefix serves to eliminate ISI and to turn the linear convolution into circular one.

2.3.2 Matrix Representation

In this section, an alternative analysis for OFDM based on a matrix representation, is illustrated [3]. The following model is realized for the transmission of a single OFDM symbol, so time instant index will not be written anymore. Initially a sequence of PSK or QAM modulated symbols are divided into blocks of length N and treated as a $N \times 1$ column vector:

$$\widehat{\boldsymbol{x}} = [\widehat{x}_1, \widehat{x}_2, \ldots, \widehat{x}_N]^T$$

and after the N-point IDFT we obtain:

$$\boldsymbol{x} = F^H \widehat{\boldsymbol{x}} = [x_1, x_2, \ldots, x_N]^T$$

Now a cyclic prefix, defined from the last $\mu+1$ samples of x, is appended at the beginning of the vector

$$\boldsymbol{x}_{cp} = [x_{-\mu}, \ldots, x_{-1}, x_0, x_1, \ldots, x_N]^T$$

This signal is convolved with the impulse response of the discrete-time channel in presence of additive white noise. The first $\mu + 1$ samples of $\boldsymbol{y}_{cp}$ are discarded and the $\boldsymbol{y}$ samples are given by:

$$\boldsymbol{y} = \widetilde{G}\boldsymbol{x}_{cp} + \boldsymbol{w} \tag{2.14}$$

where $\boldsymbol{w}$ is a vector containing iid Gaussian samples with zero mean and variance σ^2. First of all, some assumptions have to be made:

- The channel impulse response is time-invariant during the transmission of $\boldsymbol{x_{cp}}$;
- There is perfect synchronization, in time and frequency, between transmitter and receiver.
- The equivalent lowpass channel has a finite impulse response no longer than μ, i.e. there is neither ISI nor ICI

Every signal is treated as a $N \times 1$ column vector and the channel is represented by a matrix $\widetilde{G}$ of size $N \times (\mu + 1 + N)$

$$\begin{bmatrix} y_1 \\ y_2 \\ \vdots \\ y_N \end{bmatrix} = \begin{bmatrix} g_\mu & \cdots & g_1 & g_0 & & & O & & \\ & g_\mu & \cdots & g_1 & g_0 & & & O & \\ & & \ddots & & & \ddots & & & O \\ O & & & \ddots & & & \ddots & & \\ & O & & & g_\mu & \cdots & g_1 & g_0 & \\ & & O & & & g_\mu & \cdots & g_1 & g_0 \end{bmatrix} \begin{bmatrix} x_{-\mu} \\ \vdots \\ x_{-1} \\ x_0 \\ x_1 \\ \vdots \\ x_N \end{bmatrix} + \begin{bmatrix} w_1 \\ w_2 \\ \vdots \\ w_N \end{bmatrix}$$

From the construction of the cyclic prefix we know that $x_{-k} = x_{N-k}$ with $k = 0, 1 \ldots, \mu$ therefore there is some redundancy. Moreover the first μ samples are discarded to the receiver side. For instance the product between the vector $\boldsymbol{x}_{cp}$ and the first row of $\widetilde{G}$ is equal to

$$g_\mu x_{-\mu} + g_{\mu-1} x_{\mu-1} + \cdots + g_0 x_0$$

and the product between the last row of $\widetilde{G}$ and $\boldsymbol{x}_{cp}$is equal to

$$g_\mu x_{N-\mu} + g_{\mu-1} x_{N-\mu+1} + \cdots + g_0 x_N$$

Since $x_{-k} = x_{N-k}$ with $k = 0, 1 \ldots, \mu$, the last two products are equivalent, then we can reshape the matrix $\widetilde{G}$ in a square matrix G and using the vector $\boldsymbol{x}$ (without cyclic prefix). The equivalent model is given by

$$\begin{bmatrix} y_1 \\ y_2 \\ \vdots \\ y_N \end{bmatrix} = \begin{bmatrix} g_0 & & & g_\mu & \cdots & g_1 \\ g_1 & g_0 & O & & \ddots & \vdots \\ \vdots & & \ddots & O & & g_\mu \\ g_\mu & & & \ddots & O & \\ & \ddots & & & \ddots & \\ O & & g_\mu & \cdots & g_1 & g_0 \end{bmatrix} \begin{bmatrix} x_1 \\ x_2 \\ \vdots \\ x_N \end{bmatrix} + \begin{bmatrix} w_1 \\ w_2 \\ \vdots \\ w_N \end{bmatrix} = G\boldsymbol{x} + \boldsymbol{w}$$

The model above shows how the cyclic prefix insertion allows the channel to be modeled as a circulant convolution matrix over the N samples of interest. G is a normal matrix:

$$GG^H = G^H G$$

so it has an eigenvalues decomposition:

$$G = U \Lambda U^H$$

where Λ is a diagonal matrix containing the eigenvalues of G and U is a unitary matrix whose columns (or rows) constitute a set of N eigenvectors of G. Hence

$$U^H U = U U^H = I_N$$

Further from the cyclic convolution structure, G is also a circulant matrix, therefore each column is a one-step shift of the previous column. As it has been shown in [1], each column of the DFT matrix F is an eigenvector of G^T, so:

$$G^T F = F\Lambda$$

We find the channel matrix G, by multiplying F^H on each side and transposing the result.

$$G = F^H \Lambda F$$

Thus the received symbol vector $\widehat{\boldsymbol{y}} = \mathrm{DFT}(\boldsymbol{y})$ can be formulated in the frequency domain as:

$$\widehat{\boldsymbol{y}} = F\boldsymbol{y} = F\left(G\boldsymbol{x} + \boldsymbol{w}\right) = FF^H \Lambda F F^H \widehat{\boldsymbol{x}} + F\boldsymbol{w} = \Lambda\widehat{\boldsymbol{x}} + \boldsymbol{v} \tag{2.15}$$

where $\boldsymbol{v}$ is the N-point DFT of $\boldsymbol{w}$, whose elements are iid by Gaussian distribution with unitary variance and zero mean. It is seen that the received symbol vector $\widehat{\boldsymbol{y}}$ can be calculated multiplying the eigenvalues of the channel with the transmitted symbol vector $\widehat{\boldsymbol{x}}$ where each eigenvalue corresponds to each orthogonal subchannel attenuation.

2.4 OFDM Summary

In this chapter a discrete time OFDM model and an its matrix representation were presented. The robustness against multipath signal distortion and flexibility in usage of bandwidth were pointed out. For these reasons OFDM seems to be particularly suitable for transmission in multipath environment. In this chapter we assumed there is perfect synchronization in time and frequency between the transmitter and the receiver. A frequency misalignment may cause a loss of subcarrier orthogonality degrading notably the transmission quality. This effect is commonly known as *Inter-Carrier Interference* (ICI). Also synchronization in the time domain is important to avoid ISI between adjacent symbols. However in what follow, we consider neither ICI nor ISI and we assume perfect synchronization between transmitter and receiver.

Chapter 3

State-of-the-art summary

In this chapter some of state-of-the-art methods for channel estimation in OFDM systems are presented. All this methods are based on pilot assisted channel estimation (PACE) approach. A sequence of known symbols, called pilots, are systematically transmitted on the channel and used to carry out the estimation. Due to time constraints we do not use the pilot symbols configuration specified in the 3GPP setup proposed for LTE. However, if the reader is interested, a brief description is given in Appendix A. In this chapter it is explained how the channel transfer function is estimated from pilot symbol data through two different PACE algorithms. In the end, the performance of this PACE algorithms are evaluated and compared.

3.1 Channel Estimation

The signal that reach at the receiver side is distorted by the multipath channel and the additive noise. In order to recover the received symbols a channel estimation is required. In OFDM this is carried out transmitting a known sequence of symbols called pilot. Afterward, from this data a channel estimate is performed and such methods are referred as *Pilot Assisted Channel Estimation* (PACE). This approach employ only the frequency domain properties of the channel, then no use of time filtering or interpolation has been made. In this section, the state-of-the-art PACE algorithm, referred as *Robust Wiener Filter* (RWF), is compared with the *Enhanced Noise Reduction Algorithm* (ENRA) that we suppose to be a good alternative.

3.1.1 Pilot Symbol Observation

In the end of Chapter 2 it has been shown as the output vector $\widehat{\boldsymbol{y}}$ can be achieved multiplying the eigenvalues of the channel matrix by the transmitted symbol vector $\widehat{\boldsymbol{x}}$. Then recasting the equation (2.15)

$$\boldsymbol{y} = X\boldsymbol{h} + \boldsymbol{v} \tag{3.1}$$

the transfer function for the OFDM system can be equally written for the M subcarriers that are carrying pilots

$$\boldsymbol{y}_p = \boldsymbol{X}_p\boldsymbol{h}_p + \boldsymbol{v}_p$$

where $\boldsymbol{y}_p$ is the received signal at the pilot subcarriers, X_p is a diagonal matrix containing the transmitted pilots and $\boldsymbol{h}_p$ is the frequency response of the channel at the pilot frequencies. As the transmitted signal are known at the received side an initial estimate, also referred to *zero-forcing* estimate in [6], can be achieved as

$$\boldsymbol{h}_{zf} = {X_p}^{-1}\boldsymbol{y}_p = \boldsymbol{h}_p + X_p\boldsymbol{v}_p \tag{3.2}$$

where $\boldsymbol{h}_{zf}$ is known to the receiver side and $\boldsymbol{h}_p$ is the true frequency response. Once that the M complex number contained in $\boldsymbol{h_{zf}}$ are known at the receiver, we want to estimate the remaining $N_u - M$ complex number associated with subcarriers for data transmission. Then in what follow we introduce two PACE algorithms: ENRA and Robust Wiener Filter.

3.1.2 Enhanced Noise Reduction Algorithm

This channel estimator, proposed in [10], require some critical assumptions:

- the number of channel component L is assumed to be known
- the delay parameters $\boldsymbol{\tau} = [\tau_1, \tau_2, \cdots, \tau_L]$ are assumed to be known

The channel estimator model for ENRA is obtained recalling the equation (3.2) and decomposing the vector $\boldsymbol{h}_p$ as

$$\boldsymbol{h}_p = T\boldsymbol{\alpha}$$

where $\boldsymbol{\alpha} = [\alpha_1, \alpha_2, \cdots, \alpha_L]^T$ is the $L \times 1$ complex channel amplitude vector, T is an $M \times L$ Fourier matrix where each entry is given by

$$T(m,l) = e^{-j2\pi\frac{p(m)\tau_l}{\tau_s N}} \qquad m = 1, \cdots, M \quad l = 1, \cdots, L$$

Notice that the above matrix depends on the pilot symbols position and on the true delays $\boldsymbol{\tau} = [\tau_1, \tau_2, \cdots, \tau_L]$. Therefore the fundamental channel estimator model is given as

$$\boldsymbol{h}_{zf} = T\boldsymbol{\alpha} + \boldsymbol{w} \tag{3.3}$$

where $\boldsymbol{w} = {X_p}^{-1}\boldsymbol{v}_p$. The noise statistics remain unchanged because in this work has been assumed that all pilot symbols hold unit power. Then the assumption for the noise is

$$\boldsymbol{w} \sim \mathcal{CN}\left(0, \sigma_w^2 I_M\right)$$

Only the complex channel amplitude vector $\boldsymbol{\alpha}$ and the noise $\boldsymbol{w}$ are unknown terms. Then, given an estimate $\widehat{\boldsymbol{\alpha}}$ of the channel complex amplitude, the frequency response at all subcarriers is given by [10]

$$\boldsymbol{h}_{ENRA} = T_I\widehat{\boldsymbol{\alpha}} \tag{3.4}$$

where T_I is an $N_u \times L$ matrix which entries are given by

$$T(n,l) = e^{-j2\pi\frac{p(n)\tau_l}{\tau_s N}} \qquad p(n) \in \left\{-\frac{N_u}{2}, \cdots, -1, 1, \cdots, \frac{N_u}{2}\right\}$$

An estimated $\boldsymbol{\alpha}$-vector can be obtained with the theory of linear minimum mean squared error estimation, also referred as MMSE in [10]

$$\widehat{\boldsymbol{\alpha}} = \left(T^H T + \sigma_w^2 C^{-1}\right) T^H \boldsymbol{h}_{zf}$$

where C is the covariance matrix of the channel vector amplitudes. With the above estimated $\boldsymbol{\alpha}$-vector and recalling the equation (3.4) the frequency response at all active subcarriers is given by

$$\boldsymbol{h}_{ENRA} = T_I\left(T^H T + \sigma^2 C^{-1}\right)^{-1} T^H \boldsymbol{h}_{zf}$$

3.1.3 Robust Wiener Filter

As shown in literature, [10] [8], the Wiener Filter is given as

$$\boldsymbol{h}_{WF} = R_{h_I h_p}\left(R_{h_p h_p} + {\sigma_w}^2 I\right)^{-1}\widehat{\boldsymbol{h}}_p \tag{3.5}$$

where

$$R_{h_I h_p} = \mathbb{E}\left[h_I h_p^H\right] \qquad \text{and} \qquad R_{h_p h_p} = \mathbb{E}\left[h_p h_p^H\right]$$

$\boldsymbol{h}_I$ is the channel transfer function at all the N_u active subcarriers; $\boldsymbol{h}_p$ is the channel transfer function only at the M pilots position; ${\sigma_w}^2 I$ is the noise covariance matrix. In practice the two matrices $R_{h_I h_P}$, $R_{h_P h_P}$ and the noise variance ${\sigma_v}^2$ are unknown, so they

should be assumed somehow. The robust approach is derived under the assumption that the delays are mutually independent and uniformly distributed within the cyclic prefix [8]

$$\tau_l \overset{i.i.d.}{\sim} \mathcal{U}(0, \mu+1) \qquad l = 1, 2, ..., L$$

with probability distributions for the delays

$$f_{\tau_l}(\tau_l) = \begin{cases} \frac{1}{\tau_G} & \text{for} \quad 0 \leq \tau_l \leq \tau_G \\ 0 & \text{otherwise} \end{cases} \qquad 1 \leq l \leq L$$

where τ_G is the guard time. Considering the channel impulsive response introduced in (2.12), the transfer function arranged in the vector $\boldsymbol{h}_I$ read as

$$h_k = \sum_{l=1}^{L} \alpha_l e^{-j2\pi(\frac{k}{N})\tau_l} \qquad k \in \{1, \ldots, N_u\}$$

Furthermore, as suggested in [11], the total power is distributed along the L amplitude components in $\boldsymbol{\alpha}$. Considering a channel with average power normalized to unity, the power assumptions for the channel amplitudes are

$$\mathbb{E}\left[|\alpha_l|^2\right] = \frac{1}{L} \qquad l = 1, 2, \ldots, L$$

Making use of the above assumptions the Wiener filter can be applied and the two matrices in (3.5) are calculated [8]

$$\mathbb{E}[h_k h_j^*] = \frac{1 - e^{-j2\pi\tau_M \frac{k-j}{N}}}{j2\pi\tau_M \frac{k-j}{N}}$$

3.2 Performance Comparison

In this section a comparison between ENRA and RWF performance is made. The results are shown in terms of *Bit Error Rate* (BER) as a function of *Signal to Noise Ratio* (SNR). Throughout this work we always evaluate the performance in terms of SNR per bit and the modulation scheme used is a QPSK with unit power per symbol. Therefore the SNR is given as

$$\text{SNR(dB)} = 10 \log_{10} \frac{1}{2\sigma_w^2}$$

where σ_w^2 is the variance of the additive white Gaussian noise. The channel always used in the simulations is the EVA channel proposed by 3GPP in LTE standard (see Table 5.1). Another assumption that we made is the absence of ISI i.e. the maximum delay is smaller than the cyclic prefix duration. In the end a crucial assumption is

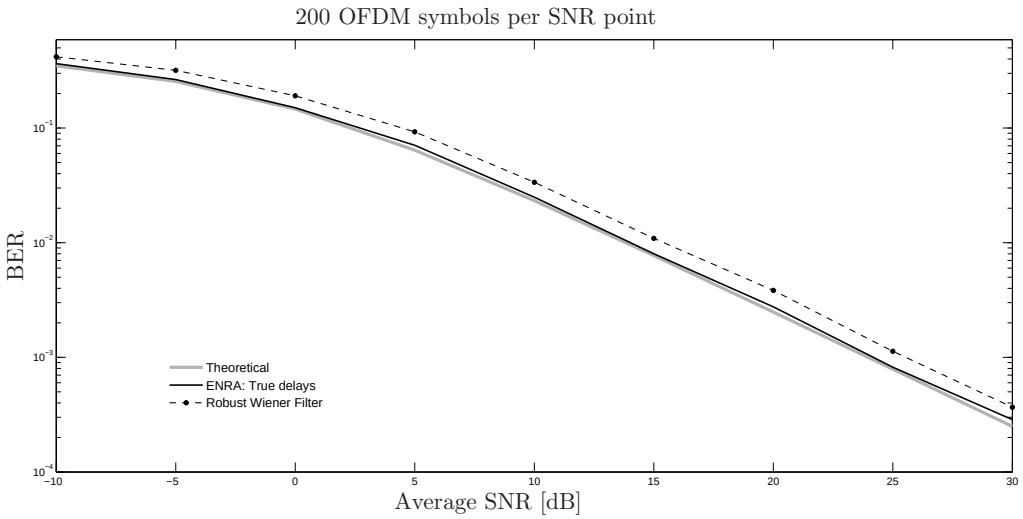

FIGURE 3.1: Performance of the ENRA with true delays compared with RWF

made on the ENRA algorithm: we assume the perfect knowledge of the multipath delay parameters. In Figure 3.1 are shown the performance of the 2 PACE algorithms. The results show that both ENRA and RWF performance improve as the SNR increases. Furthermore, the ENRA outperform the RWF, being really close to the theoretical limit. However remember that this algorithm is provided with perfect a priori channel knowledge, contrariwise the RWF does not require any information. The multipath delay parameters are not known in practice, therefore they have to be estimated if we want to use the ENRA algorithm. Furthermore , especially for high SNR values, erroneous estimates of delays cause a notably performance degrading. In the remaining part of the thesis we focus our attention on the multipath delays parameters estimation.

Chapter 4

Beamforming

Historically, beamforming is a signal processing technique used to automatically localize a signal source coming from small non-directional array forming a single directional beam [12]. A variety of methods adopted for this estimation problem are well consolidated in literature and in [1] and [2] have been investigated for tap-delay estimation in multipath environment. These works have shown that a recursive version of beamforming, called *Sequential Beamforming Algorithm* (SBA), seems to give interesting results for the tap-delay estimation in a multipath channel. Furthermore the complexity of the SBA is low compared to the other investigated methods because only one dimensional search grid is required to perform the estimate of each delay. In what follow the beamforming technique is presented and some improvements about SBA are investigated.

4.1 Framework and assumptions

The problem of central interest in this chapter, is that of estimating the delay vector $\boldsymbol{\tau}(k)$ using a beamforming methods for a given finite set of $\boldsymbol{h}_{zf}(k)$. The receiver memorizes a set of K zero-forcing estimates in the $M \times K$ matrix

$$H_{zf} = \begin{bmatrix} | & | & & | \\ \boldsymbol{h}_{zf}(1) & \boldsymbol{h}_{zf}(2) & \dots & \boldsymbol{h}_{zf}(K) \\ | & | & & | \end{bmatrix}$$

For each vector we consider the observation model:

$$\boldsymbol{h}_{zf}(k) = T(\boldsymbol{\tau}(k))\boldsymbol{\alpha}(k) + \boldsymbol{n}(k) \qquad k = 1, \dots, K \tag{4.1}$$

where k is a time index. The channel amplitude vector can be considered unknown but fixed and the statistics of the vector observation is:

$$\boldsymbol{h}_{zf}(k) \sim \mathcal{CN}\left(T(\boldsymbol{\tau}(k))\boldsymbol{\alpha}(k), \sigma^2 I_M\right), \qquad k = 1, 2, \ldots, K$$

In this case, the only random contribution is due to the noise that is assumed to be complex Gaussian and spatially and temporally uncorrelated. This mean that the noise has the same variance σ^2 and it is uncorrelated among all M pilot subcarriers. Furthermore, the noise is uncorrelated between all snap-shots collected at each time instant k. Another fundamental assumption is made on the number of the attending delay. That is, we assume $L(t) = L$ to stay fixed during the time span under consideration. Then we consider the channel time-invariant during that time interval. In [13] some techniques for estimating the number of signal, if such information is not available, have been investigated. The matrix $T(\boldsymbol{\tau}(k))$ in the observation model (4.1) is defined as

$$T(\boldsymbol{\tau}(k)) = \begin{bmatrix} | & | & & | \\ \boldsymbol{t}(\tau_1(k)) & \boldsymbol{t}(\tau_2(k)) & \cdots & \boldsymbol{t}(\tau_L(k)) \\ | & | & & | \end{bmatrix}$$

and each column vector is given by:

$$\boldsymbol{t}(\tau) = \begin{bmatrix} e^{-j2\pi p(1)\tau_i/N} & e^{-j2\pi p(2)\tau_i/N} & \ldots & e^{-j2\pi p(M)\tau_i/N} \end{bmatrix}^T \qquad i = 1, 2, \ldots, L$$

It's evident that the knowledge of the true delays is needed to build the above matrix. The purpose of this work is precisely to estimate the true delays τ_i. In this chapter, in order to solve this estimation problem, we use a filterbank approach and a *Finite Impulse Response* (FIR) filter is designed. This method is called beamforming and the filter output is given by

$$y(k) = \sum_{m=1}^{M} w_m^* h_m(k) = \boldsymbol{w}^H \boldsymbol{h}_{zf}(k)$$

where $h_m(k)$ are the M coefficients zero-forcing estimated and $\boldsymbol{w}$ is a vector containing the FIR filter coefficients (* represents the complex conjugate, used in order to simplify notation). The beamformer output, shown in Figure 4.1, is a linear combination of the M coefficients zero-forcing estimated and $\boldsymbol{w}$ is a weighting vector. The beamforming output depends on the matrix $T(\boldsymbol{\tau}(k))$ and therefore on the true delays τ_i. The vector $\boldsymbol{w}$ is designed such that the output FIR power is maximum for the true delays. Then

the empirical average power is calculated as

$$P(\boldsymbol{w}) = \frac{1}{K}\sum_{k=1}^{K} |\boldsymbol{w}^H \boldsymbol{h}_{zf}(k)|^2 = \boldsymbol{w}^H R \boldsymbol{w} = \frac{1}{K}\|\boldsymbol{w}^H H_{zf}\|^2 \tag{4.2}$$

where we have introduced the *sample covariance matrix*

$$R := \frac{1}{K}\sum_{k=1}^{K} \boldsymbol{h}_{zf}(k)\boldsymbol{h}_{zf}^H(k) = \frac{1}{K} H_{zf} H_{zf}^H \tag{4.3}$$

The problem of maximizing the output power is solved through different approaches. One is the *Conventional Beamforming* which will be described in the next section.

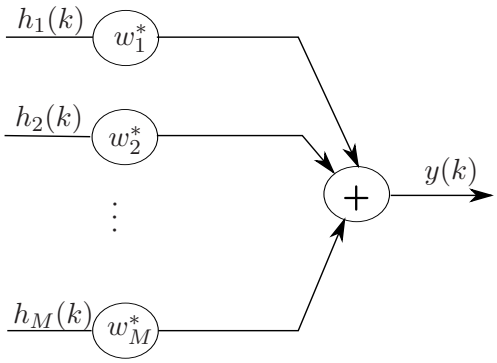

FIGURE 4.1: A beamformer forms a linear combination of the M coefficients h_m

4.2 Conventional Beamformer

The conventional beamformer is an algorithm that maximizes the output power defined in (4.2) for a given input observation vector. Let consider a channel with only one delay. We want to maximize the output power in terms of this signal delay only. Then, for a given complex amplitude α_1, and its associated delay τ_1, the zero-forcing estimation is:

$$\boldsymbol{h}_{zf} = \boldsymbol{t}(\tau_1)\alpha_1 + \boldsymbol{n}$$

We can formulate the maximization power criterion as:

$$\begin{aligned} \max_{\boldsymbol{w}} \mathbb{E}\left[|\boldsymbol{w}^H \boldsymbol{h}_{zf}|^2\right] &= \max_{\boldsymbol{w}} \boldsymbol{w}^H \left(|\alpha_1|^2 \boldsymbol{t}(\tau_1)\boldsymbol{t}^H(\tau_1) + \mathbb{E}[\boldsymbol{n}\boldsymbol{n}^H]\right)\boldsymbol{w} \\ &= \max_{\boldsymbol{w}} |\boldsymbol{w}^H \boldsymbol{t}(\tau_1)|^2 \end{aligned} \tag{4.4}$$

To avoid that the norm of $\boldsymbol{w}$ is unnecessary large it is constrained to $\|\boldsymbol{w}\| = 1$. Therefore, the scalar product $|\boldsymbol{w}^H \boldsymbol{t}(\tau_1)|$ in (4.4) is maximum when $\boldsymbol{w}$ is chosen proportional to $\boldsymbol{t}(\tau_1)$

(**Cauchy-Schwartz inequality**, [14]). Then, the unique solution is

$$\boldsymbol{w}_{bf} = \frac{\boldsymbol{t}(\tau_1)}{\|\boldsymbol{t}(\tau_1)\|} \tag{4.5}$$

Of course the true delay τ_1 is unknown, but (4.5) guarantee that the empirical average power in (4.2) will peak for $\tau = \tau_1$. Considering a channel with L delays and neglecting the cross-terms, the maximization problem become

$$\max_{\boldsymbol{w}} \left[|\boldsymbol{w}^H \boldsymbol{t}(\tau_1)|^2 + |\boldsymbol{w}^H \boldsymbol{t}(\tau_2)|^2 + \cdots + |\boldsymbol{w}^H \boldsymbol{t}(\tau_L)|^2 \right]$$

and

$$\boldsymbol{w}(\tau) = \frac{\boldsymbol{t}(\tau)}{\|\boldsymbol{t}(\tau)\|}$$

The weighting vector depends on τ and the value of the output power, as in (4.2), should give a peak for each $\tau = \tau_i$. Then the estimation problem can be carried out performing a grid-search and selecting, as a estimated delays, the value of τ that give a peak in the average empirical power. In the following, an algorithm for peak detection is introduced but we will see that its implementation is a task far from trivial. It's clearly visible that the weighting vector not depends on the actual observation, i.e. the vector $\boldsymbol{h}_{zf}$. The expression for the conventional beamformer is obtained entering the above choice of $\boldsymbol{w}$ in (4.2)

$$P_{BF}(\tau) = \frac{\|\boldsymbol{t}^H(\tau) H_{zf}\|^2}{K\|\boldsymbol{t}(\tau)\|^2} \tag{4.6}$$

In [1] is shown, by simulation, that the beamforming algorithm's performances is almost identical for different values of the snapshot memory K. Then in order to relieve the computational task, a single snapshot can be considered:

$$P_{BF}(\tau) = \frac{|\boldsymbol{t}^H(\tau)\boldsymbol{h}_{zf}|^2}{\|\boldsymbol{t}(\tau)\|^2} \tag{4.7}$$

This equation gives a good indication of the energy associated to each value of delay and should peak at the true delays. The maximization is approximated from direct numerical examination e.g. grid search.

In Figure 4.2, a beamforming spectrum normalized to the maximum value is qualitatively shown. The graphics point out as beamforming suffers from high side lobes that might be incorrectly identified as a maximum, i.e. as a delay. Then the implementation of this maximization problem, in a calculator, is going to be tricky. Furthermore the wide main lobes might hide smaller peaks implying that closely delays can not be separated by the beamformer. For instance, the last delay in the figure above will not be detected because masked by noise and side lobes.

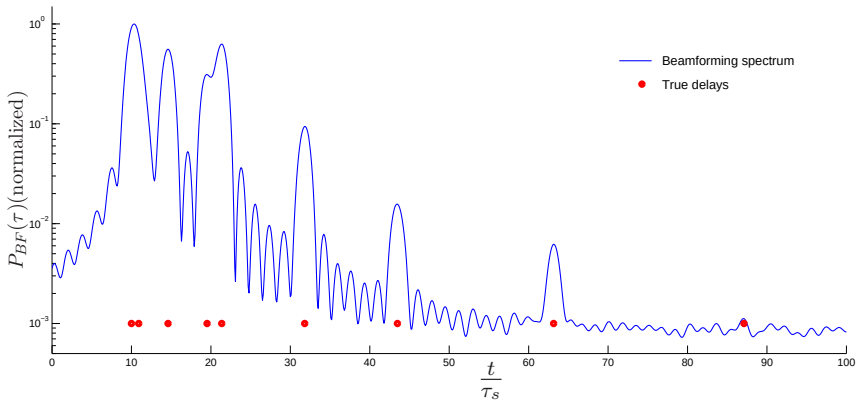

FIGURE 4.2: Normalized Beamforming Spectrum, 10 dB SNR, 200 snap-shots

4.3 Capon Beamformer

The Capon's beamformer is presented in order to improve the minimum resolution in tap-delay separation imposed in the above beamformer [12, 14]. Another choice for the weighting vector is obtained imposing in (4.2) the following optimization problem:

$$\min_{\boldsymbol{w}} P(\boldsymbol{w}) \qquad \text{subject to} \qquad \boldsymbol{w}^H \boldsymbol{t}(\tau) = 1 \tag{4.8}$$

Intuitively, (4.8) attempts to minimize the average power for all delay values except for the particular delay τ under observation, that should keep a fixed gain. The solution to (4.8), as derived in [14] is given by:

$$\boldsymbol{w}_{capon} = \frac{R^{-1}\boldsymbol{t}(\tau)}{\boldsymbol{t}^H(\tau)R^{-1}\boldsymbol{t}(\tau)}$$

The weighting vector associated to the Capon beamformer, unlike the conventional beamformer, depends on the actual observation. Inserting the above solution into (4.2):

$$P_{capon}(\tau) = \boldsymbol{w}_{capon}^H R \boldsymbol{w}_{capon} = \frac{1}{\boldsymbol{t}^H(\tau)R^{-1}\boldsymbol{t}(\tau)} \tag{4.9}$$

In Figure 4.3 a Capon beamforming spectrum normalized to the maximum value is shown. The graphics is obtained from 200 observations and a SNR of 10 dB. It is observed that Capon has higher minimum resolution cause it has narrow peaks and no significant side lobs. But the computational complexity is higher because a matrix inversion is required. It has been assumed the existence of the matrix inverse implying that the covariance matrix is full rank. This assumption sets a minimum limit on the amount of observation needed for avoid a singular covariance matrix.
Considering the theorem of the rank of a matrix product [14] and recalling the sample

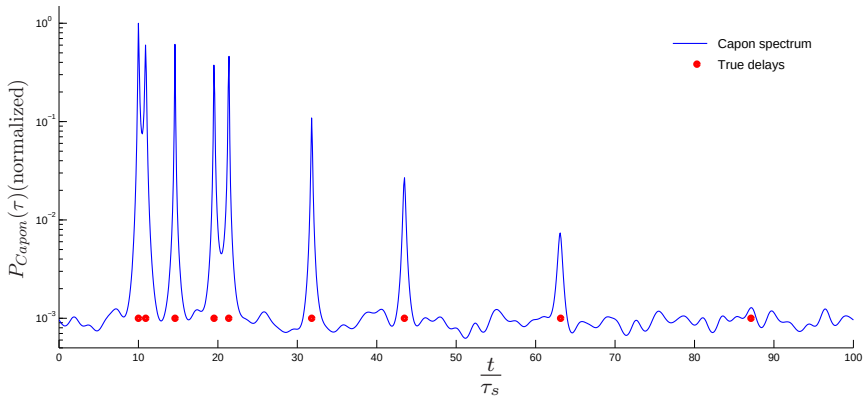

FIGURE 4.3: Normalized Capon's spectrum, 10 dB SNR, 200 snap-shots

covariance matrix (4.3)

$$\underset{(M\times M)}{rank(R)} \leq \underset{(M\times K)}{rank(H_{zf})}$$

It's evident that the sample covariance matrix can be a full rank matrix only if $K \geq M$, i.e. the number of collected snap-shots is bigger than the number of row in the matrix H_{zf}

4.4 SBA

In this section a sequential beamforming algorithm is presented [9] [1]. It is based on an iterative technique that transforms the L-dimensional optimization procedure, needed for the conventional beamforming, into a sequence of L much simpler one-dimensional searches. At every iteration a maximization is performed with respect to a single delay and a projection operator is recursively constructed. Recalling (4.7) the first delay is given by

$$\widehat{\tau}_1 = \arg\max_{\tau} \left\{ \frac{\left|\boldsymbol{t}^H(\tau)\boldsymbol{h}_{zf}\right|^2}{\left\|\boldsymbol{t}(\tau)\right\|^2} \right\}$$

The value of τ that gives the maximum in the above equation is found performing a search grid. Then τ is sampled and the beamforming value is calculated for a finite set of value. When a delay is found we have to search in a subspace orthogonal to $\boldsymbol{t}(\widehat{\tau}_1)$. Then the initial projection operator is constructed

$$\Pi_1(\widehat{\tau}_1) = \frac{\boldsymbol{t}(\widehat{\tau}_1)\boldsymbol{t}^H(\widehat{\tau}_1)}{\left\|\boldsymbol{t}(\widehat{\tau}_1)\right\|^2}$$

Hereby, $\boldsymbol{t}(\tau)$ is projected on the orthogonal complement of the above projection operator:

$$\boldsymbol{t}_1(\tau) = \boldsymbol{t}(\tau) - \Pi_1(\widehat{\tau}_1)\boldsymbol{t}(\tau)$$

This operation act on the Beamforming spectrum shutting down the peak due to the delay $\widehat{\tau}_1$, as shown in Figure 4.4. Then a new delay can be estimated by:

$$\widehat{\tau}_2 = \arg\max_{\tau} \left\{ \frac{\left| \boldsymbol{t}_1^H(\tau) \boldsymbol{h}_{zf} \right|^2}{\left\| \boldsymbol{t}_1(\tau) \right\|^2} \right\}$$

For searching after additional delay it is needed to update the projection operator. To relieve the computational load at each iteration, we introduce the following projection matrix property [9]

$$\Pi_2(\widehat{\tau}_2; \widehat{\tau}_1) = \Pi_1(\widehat{\tau}_1) + \frac{\boldsymbol{t}_1(\widehat{\tau}_2)\boldsymbol{t}_1^H(\widehat{\tau}_2)}{\left\| \boldsymbol{t}_1(\widehat{\tau}_2) \right\|^2}$$

Then $\boldsymbol{t}_2(\tau)$ is projected on the orthogonal complement of the current projection operator $\Pi_2(\widehat{\tau}_2, \widehat{\tau}_1)$. The above procedure is repeated until a specific number of delays are collected. In Figure 4.4 the first three iteration of the sequential beamforming algorithm are shown. The graphic has been obtained using only one snap-shot and 10 dB of SNR. The x-asis is included in $(0, 100)$ and the sampling step is 0.1 therefore 1000 sample have been used. It show how the projection operator shut down the peaks after each delay detection.

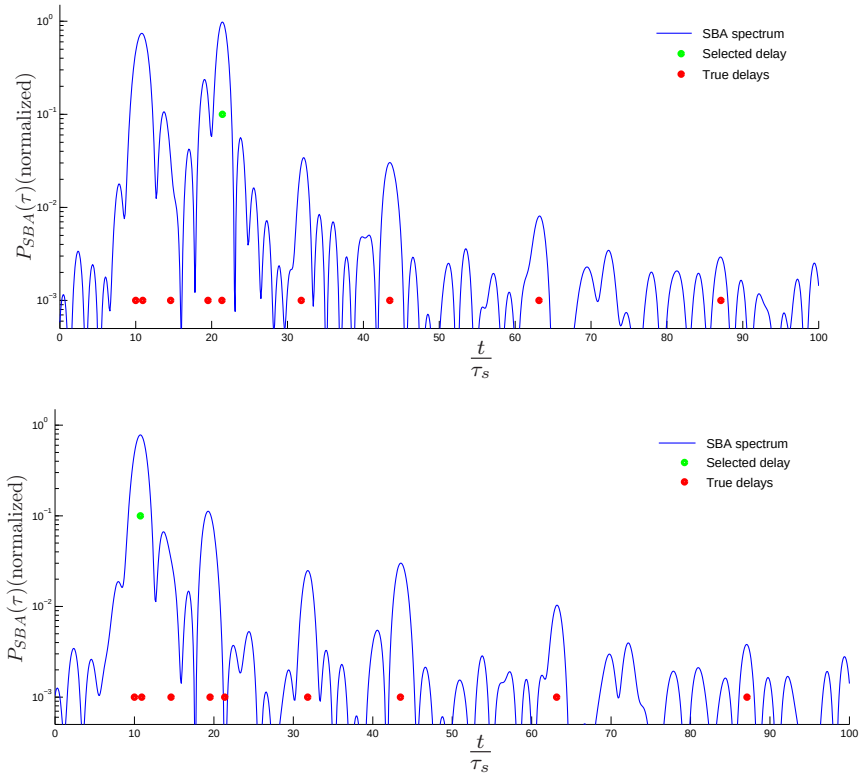

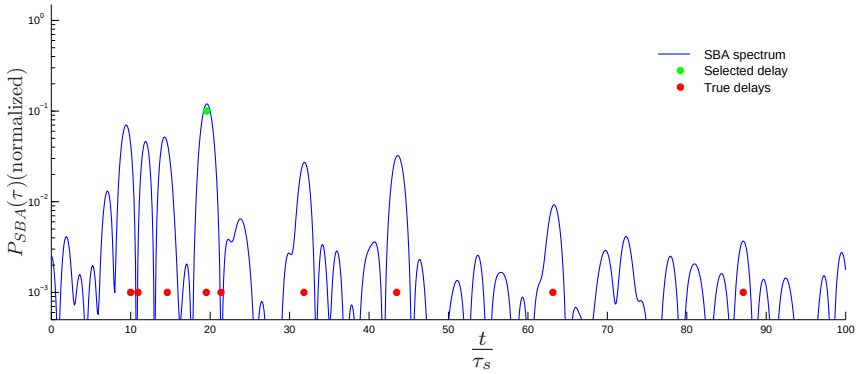

FIGURE 4.4: Sequential Beamforming Algorithm, three iterations

4.5 SBA Features

Three methods have been compared in this chapter: Conventional beamforming, Capon beamforming and Sequential beamforming. The first one can be carried out with only one snap-shot available and the computational load is lower, but it suffer from high side lobes and its implementation in calculator is a task far from trivial. The Capon beamforming gave a good power spectrum allowing higher minimum resolution due to the narrow peaks. The main drawback is that huge matrix inversions are required, therefore it is more computational complex. The last algorithm analyzed is the SBA that we believe to be the best compromise between complexity and minimum resolution. Furthermore, SBA has some interesting properties that can be pointed out analyzing the beamforming power spectrum. In order to analyze the beamforming power let consider a scaled version of $\boldsymbol{t}(\tau)$

$$\boldsymbol{\beta}(\tau) = e^{-j2\pi p(1)\frac{\tau}{N}}\boldsymbol{t}(\tau) = \begin{bmatrix} 1 & e^{-j2\pi\frac{\gamma\tau}{N}} & e^{-j2\pi\frac{2\gamma\tau}{N}} & \cdots & e^{-j2\pi\frac{\gamma(M-1)\tau}{N}} \end{bmatrix}^T$$

where M indicate the number of subchannels used for pilot symbols and γ is the spacing between two pilot subcarriers. Let recast the inner product in (4.4)

$$\left|\boldsymbol{w}^H\boldsymbol{t}(\tau_1)\right|^2 = \left|\frac{\boldsymbol{\beta}^H(\tau)\boldsymbol{\beta}(\tau_1)}{\|\boldsymbol{\beta}(\tau)\|}\right|^2 \tag{4.10}$$

As earlier mentioned for this choice of weighting vector, the maximum is given when $\tau = \tau_1$. It could be interesting to see what happen when the gap $\Delta\tau$, between τ and τ_1 is changed. Then neglecting the constant terms, the following function is defined

$$z(\Delta\tau; M, N, \gamma) = \left|\boldsymbol{\beta}^H(\tau)\boldsymbol{\beta}(\tau+\Delta\tau)\right|^2 = \left|\sum_{m=0}^{M-1} e^{-j2\pi\gamma\frac{m\Delta\tau}{N}}\right|^2 \tag{4.11}$$

where $z(\Delta\tau; M, N, \gamma)$ rely only on $\Delta\tau$. The function, shown in Figure 4.5, has been

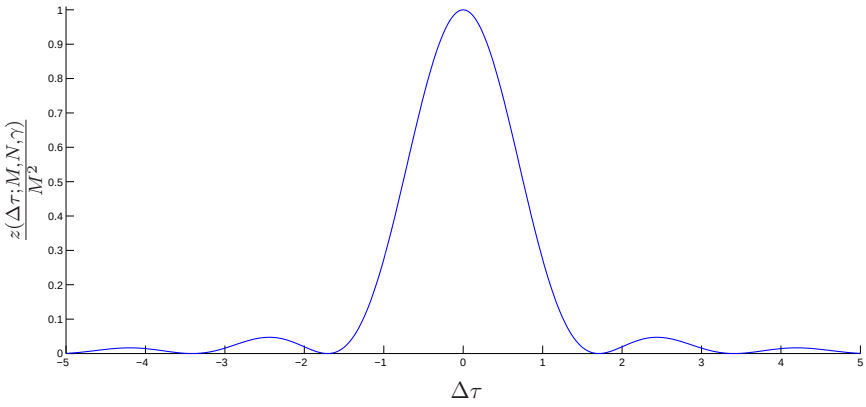

FIGURE 4.5: $z(\Delta\tau; M, N, \gamma)$ obtained with LTE parameters ($M = 200$, $N = 2048$, $\gamma = 6$). The function is normalized to the maximum value M^2 and the main lobe width is 3.4 $\frac{t}{\tau_s}$ in LTE setup

obtained with the LTE parameters defined in Table A.1 and it is normalized to the maximum value M^2. The main lobe width can be found by setting the equation (4.11) equal to zero and solving with respect to $\Delta\tau$.

$$\phi = 2\,\frac{N}{\gamma\,M} = 2\,\frac{N}{N_u}$$

Then, for a given number of subchannels and active subchannels, we can not manipulate the main lobe width, but we can only higher the peak value increasing M. Obviously, in this case, the pilot subcarrier spacing has to be decreased. Bearing in mind what above, the empirical average power can be written as:

$$\left|\boldsymbol{\beta}^H(\tau)\boldsymbol{h}_{zf}\right|^2 = \sum_{l=1}^{L} |\alpha_l|^2 \left|\boldsymbol{\beta}^H(\tau)\boldsymbol{\beta}(\tau_l)\right|^2 + \left|\boldsymbol{\beta}^H(\tau)\boldsymbol{n}\right|^2 + \Omega$$

where all the cross-terms have been collected in

$$\Omega = \sum_{l=1}^{L}\sum_{\substack{k=1\\k\neq l}}^{L} \boldsymbol{\beta}^H(\tau)\boldsymbol{\beta}(\tau_l)\boldsymbol{\beta}^T(\tau)\boldsymbol{\beta}^*(\tau_k)\alpha_l\alpha_k^* + \sum_{l=1}^{L} 2\Re\left\{\boldsymbol{\beta}^H(\tau)\boldsymbol{\beta}(\tau_l)\boldsymbol{\beta}^T(\tau)\boldsymbol{n}^*\alpha_l\right\}$$

As shown in Figure 4.6, the most important contribution to the beamforming power is given by

$$C(\tau) = \sum_{l=1}^{L} |\alpha_l|^2 \left|\boldsymbol{\beta}^H(\tau)\boldsymbol{\beta}(\tau_l)\right|^2$$

where the inner product is the same shown in (4.11). Then $C(\tau)$ is merely a sum of $z(\Delta\tau; M, N, \gamma)$ functions shifted on each true delay and multiplied by the complex amplitude absolute value to the square.

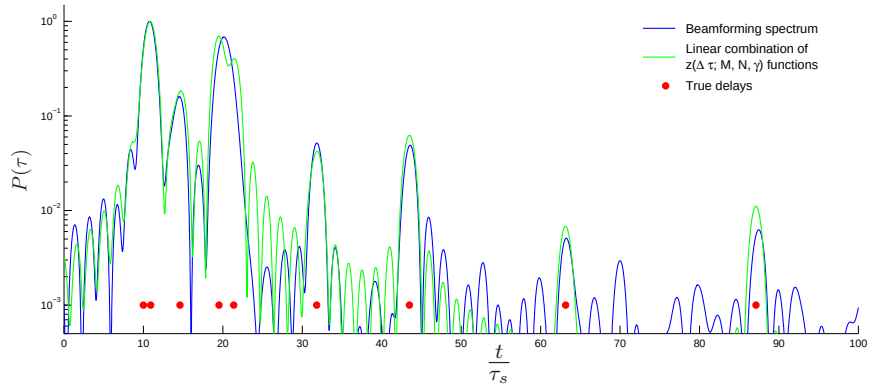

FIGURE 4.6: Beamforming output compared to a linear combination of $z(\Delta\tau; M, N, \gamma)$ functions

4.6 Beamforming Summary

The algorithms investigated in this chapter are: Conventional Beamformer, Capon Beamformer and Sequential Beamformer Algorithm. The former has a low computational load but suffers from high sides lobe. The Capon is introduced in order to improve the resolution in the search depth. The major drawback of this algorithm is that it requires the sample covariance matrix to be invertible. Hence an huge amount of observations is needed for guarantee the matrix inverse existence. Whereas, the SBA requires only the current observations i.e. no memory needed and the computational complexity is lower compared to the Capon Beamformer. Furthermore, some interesting properties of this algorithm have been shown in the latter section. Then, in the remaining part of this thesis, we consider and investigate only the SBA algorithm.

Chapter 5

Simulations and Results

In this chapter, the sequential beamforming algorithm is evaluated through a simulation study. The delays provided by this algorithm are plugged into ENRA presented in Chapter 3, and the performance are compared to the RWF and the known channel. The performance are evaluated in terms of *Bit-Error-Rate* (BER) for different values of *Signal-to-Noise-Ratio* (SNR). It is demonstrated that SBA could be a reasonable candidate against the RWF. The simulations are carried out looking at the theory discussed in Chapter 2, 3, 4. In the first part of this chapter the LTE reference channel and the simulation setup is illustrated. Afterwards we try to find a trade-off between complexity and performance acting on some key parameters like the number of delay or the grid search resolution. In the end there is a discussion about the results obtained.

5.1 Simulation setup

In order to evaluate the performance of an algorithm that will detect the multipath delays we need to define a mutipath channel model. In this work has been assumed the absence of a component in *Line-of-Sight*(LOS) i.e. a Rayleigh fading channel model is assumed. In [15] three different multipath profiles are proposed by 3GPP in the LTE standard:

- Extended Pedestrian A model (EPA) with maximum excess delay of $410ns$
- Extended Vehicular A model (EVA) with maximum excess delay of $2510ns$
- Extended Typical Urban (ETU) with maximum excess delay of $5000ns$

Only in the last model there are some degree of ISI because the maximum excess delay is bigger then the duration of cyclic prefix. However in this work it has been assumed

that there are no ICI no ISI, and the model considered for simulations is the Extended Vehicular (EVA). The delays profile and the power relative to this channel are shown in Table 5.1

Delays (ns)	Relative Power $[dB]$
0	0.0
30	-1.5
150	-1.4
310	-3.6
370	-0.6
710	-9.1
1090	-7.0
1730	-12.0
2510	-16.9

TABLE 5.1: Extended Vehicular A model (by 3GPP)

As it has been assumed previously, the number of delays is kept fixed and in this channel it has been chosen equal to nine. Another assumption that we made is the perfect synchronization in time and frequency, between transmitter and receiver. A time guard interval is needed to the receiver side, in order to carry out the synchronization procedure. Then, the entire delays profile is shifted by an amount of ten samples to the right of zero in order to imitate the time guard interval. This profile is shown in Table 5.2

Tap-delay $(\frac{t}{\tau_s})$	Relative Power $[dB]$
10	0.0
10.92	-1.5
14.61	-1.4
19.52	-3.6
21.37	-0.6
31.81	-9.1
43.49	-7.0
63.15	-12.0
87.11	-16.9

TABLE 5.2: Extended Vehicular A profile shifted 10 sample to right of zero

The simulator is based on the theory studied in the previous chapter. The scripts forming the simulator has been provided by the NAVCOM section of Aalborg University and the main steps are illustrated in Figure 5.2. The LTE specifications are used as parameters but the pilot pattern is not used in order to simply the simulator and to make it as intuitive as possible. In fact we assume that pilots are inserted in every OFDM symbols and not only in the first and fifth of each slot as described in Appendix A. The pilots are all spaced by 6 symbols with an initial indent equal to 3 (this pattern is shown in Figure 5.1).

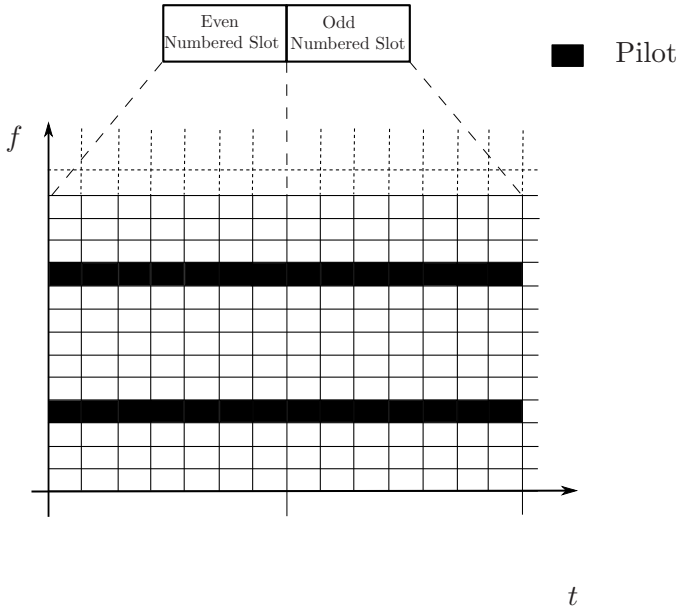

FIGURE 5.1: Pilot pattern used in the simulator. It is different from the pattern specified by 3GPP for simplify the simulator

In the main loop, data bits are randomly generated and modulated to QPSK symbols. Afterward they are transmitted in a channel designed accordingly to the OFDM system model presented in (3.1). Therefore noise and multipath corruption are added. Then, through the zero forcing estimate, the channel transfer function at the M pilot subcarrier is obtained

$$\boldsymbol{h}_{zf} = {X_p}^{-1}\boldsymbol{y}_p$$

The frequency response at all subcarriers position is estimated with Robust Wiener Filter and ENRA. For the latter it is needed to know the delays, therefore the SBA is applied. In order to detecting the peaks produced by the tap-delays a peak search is needed. The peak detection is performed through a grid obtained sampling the time line. Very important is the choice of the sampling time i.e. the grid-search resolution, because it is proportional to the computational complexity. In fact for high resolution, complexity become much more high compared to the RWF. In the next section the SBA is investigated focusing on the grid-search resolution and a trade-off between computational complexity and search depth is found.

5.2 Grid Search Sampling

In our simulator the peak detection is carried out in the interval $[0, 100]\frac{t}{\tau_s}$. That is because we know in the EVA channel where the delay are positioned. In an actual system a different interval should be considered in order to capture all the delays. In

what follow the SBA performance are shown for different value of grid-search resolution in terms of *Bit-Error-Rate* (BER) in Figure 5.3 and in terms of *Mean Square Error* (MSE) in Figure 5.4.

Both of the figures point out how the performance get better increasing the grid-search resolution. Furthermore we figured out by simulations, that keep increasing the resolution does not significantly improves the SBA performance. For this reason we consider the lowest curve (resolution 0.1) as a sort of lower bound that can not be notably improved by incrementing the grid search resolution. The most important drawback coming by the use of high resolution is the computational complexity. In fact using the highest resolution and sampling in $[0, 100]\frac{t}{\tau_s}$ require an heavy computational load. In

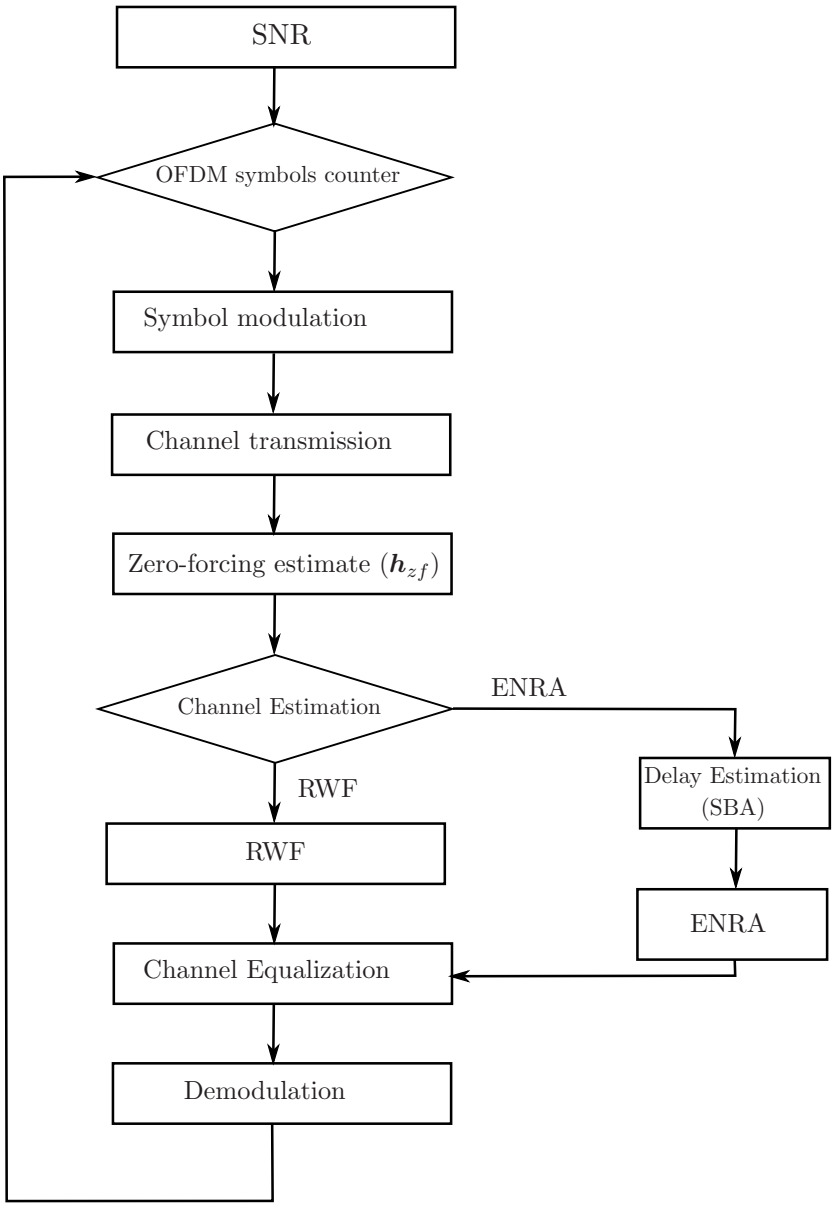

FIGURE 5.2: Structure of the used simulator

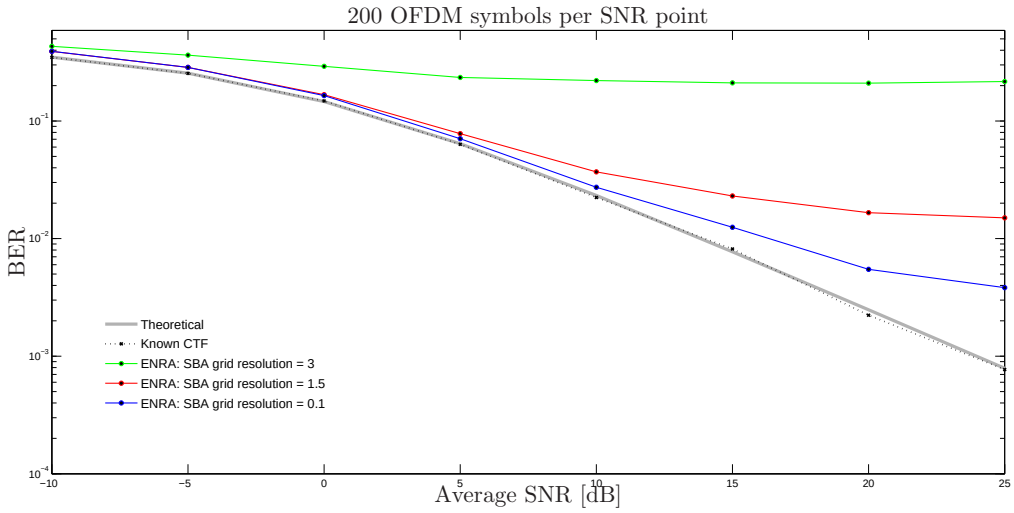

FIGURE 5.3: BER for different value of grid resolution

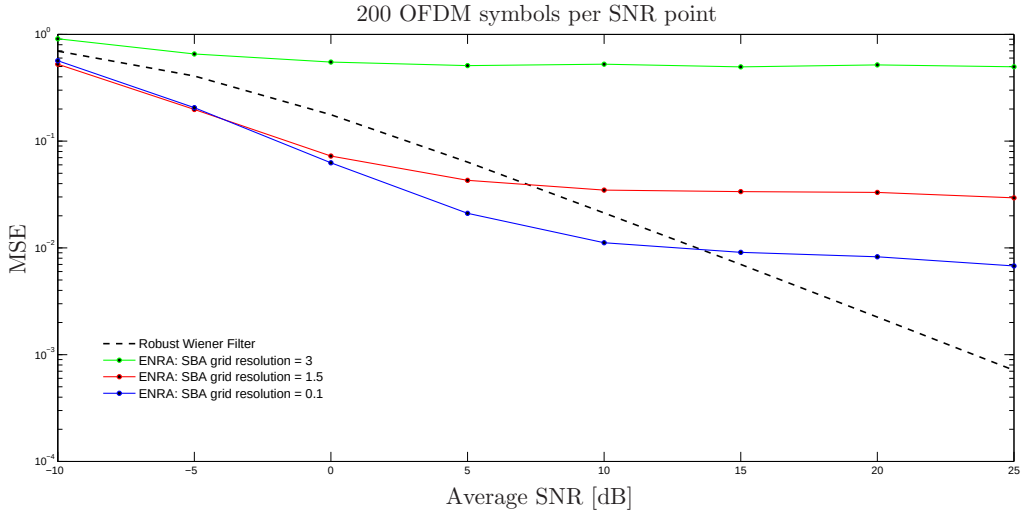

FIGURE 5.4: MSE for different value of grid resolution

order to lower the complexity without degrading the algorithm performance some ideas are presented and investigated in the following sections.

5.2.1 Parabola approximation

This method is based on the assumption that the peak can be approximated by a parabola function (see Figure 4.5). Given tree points the coefficients for the parabola equation

$$y = ax^2 + bx + c$$

can be found. Then the maximum is given by $-\frac{b}{2a}$.

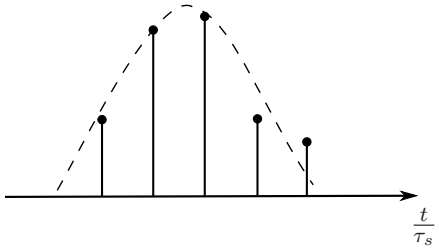

FIGURE 5.5: Parabola approximation

The results obtained using this method are shown in Figure 5.6 in terms of BER per SNR value. Although it seems to be a valid solution, cause it provides continuous resolution

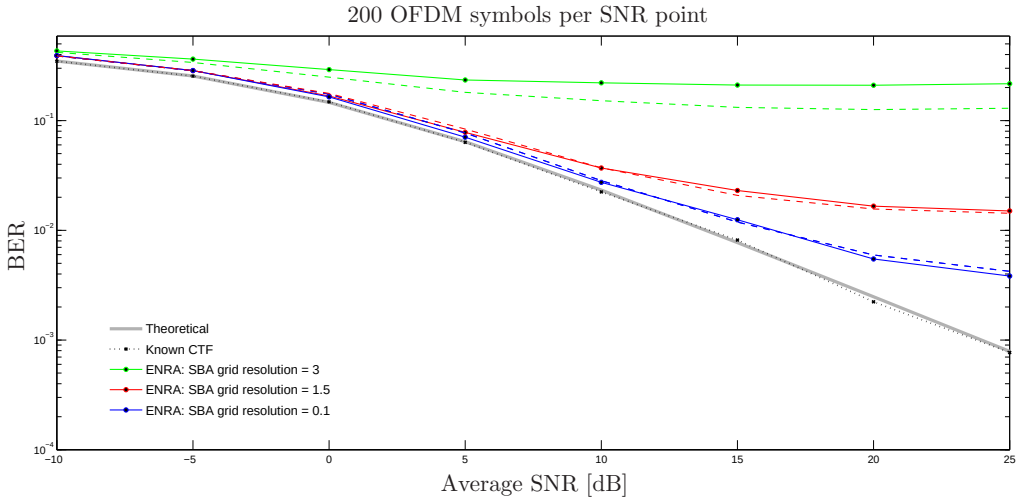

FIGURE 5.6: BER for different value of resolution. The dotted lines represent the results obtained using the parabola approximation

on the delay axis, the simulation results are not satisfying. As visible in the plot, it can improve only the worst resolution keeping unchanged the performance for the higher resolution.

5.2.2 Left/right search

This grid search is an iterative method that can be performed until a pre-specified resolution is achieved. This is done after the first rough grid-search. Given the maximum derived by the first rough search, one left and one right side samples are selected. Afterward the smallest is discarded and a new sample is created between the two currents one. This iterative procedure is repeated until the required accuracy is reached. As earlier mentioned, the resolution equal to 0.1 can be considered as a kind of lower bound because further increment can not notably improves the performance. Table 5.3 show how many iterations are needed for reach the desired accuracy starting from the rough resolutions equal to 1.5 and 3. In Figure 5.8 are shown the results obtained using this

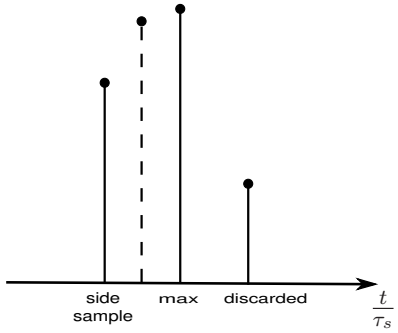

FIGURE 5.7: The left/right search method

method for different value of iterations number in terms of BER per SNR value. The final accuracy is 0.1 because incrementing it the performance does not improve significantly. Obviously it does not make sense to apply the left/right method for the highest resolution cause it is already enough depth. Starting from a resolution equal to 1.5 and with final accuracy equal to 0.1 the performance are very close to our lower bound but with lower computational complexity. In fact we need to process a number of samples one order of magnitude smaller then if we apply direct the SBA with resolution equal to 0.1. In conclusion we believe that the best trade-off between accuracy and computational complexity is to use the left/right method with accuracy equal to 0.1 and initial resolution equal to 1.5.

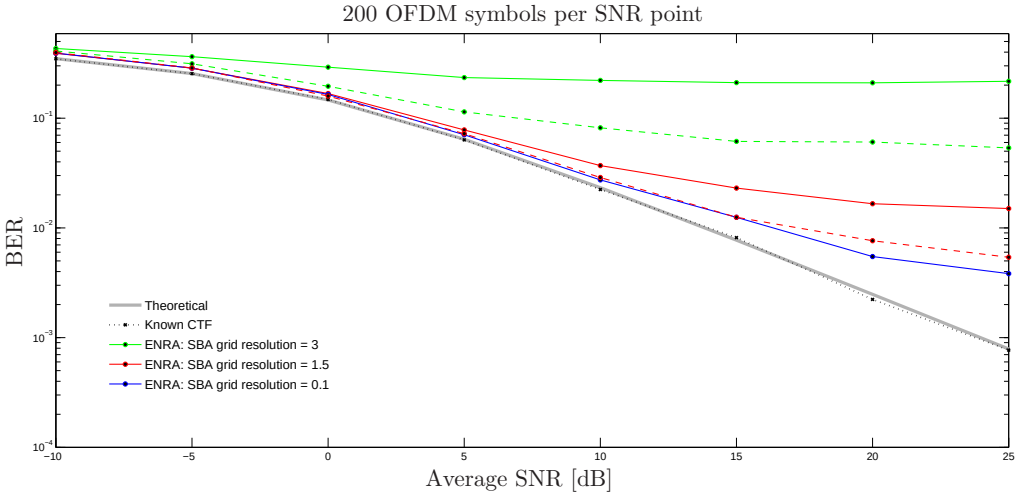

FIGURE 5.8: BER for different value of the first grid resolution with a final accuracy equal to $0.1\frac{t}{\tau_s}$. The dotted lines represent the results obtained using the left/right approximation

Rough grid $(\frac{t}{\tau_s})$	1st iteration	2nd iteration	3rd iteration	4th iteration	5th iteration
3	1.5	0.75	0.37	0.18	0.09
1.5	0.75	0.37	0.18	0.09	0.045

TABLE 5.3: Accuracy and number of iteration

5.3 The Number Of Delays

As shown in Section 2.2.1, the multipath channel is characterized by a time variant impulse response, then the delays parameters change over time. Usually, in mobile communication links the multipath delays parameters $\tau_l(t)$, $l = 1, 2, \ldots, L(t)$, are slowly time-varying compared to the amplitude and phase terms. Hence, when we consider a short time windows we may assume $L(t) = L$ and $\tau_l(t) = \tau_l$ as static and deterministic terms. The simulations are carried out using the EVA channel with nine delays, proposed by 3GPP in the LTE standard. The knowledge of this number is underlying for carry out the SBA algorithm. In Figure 5.9 are shown the performance of SBA collecting

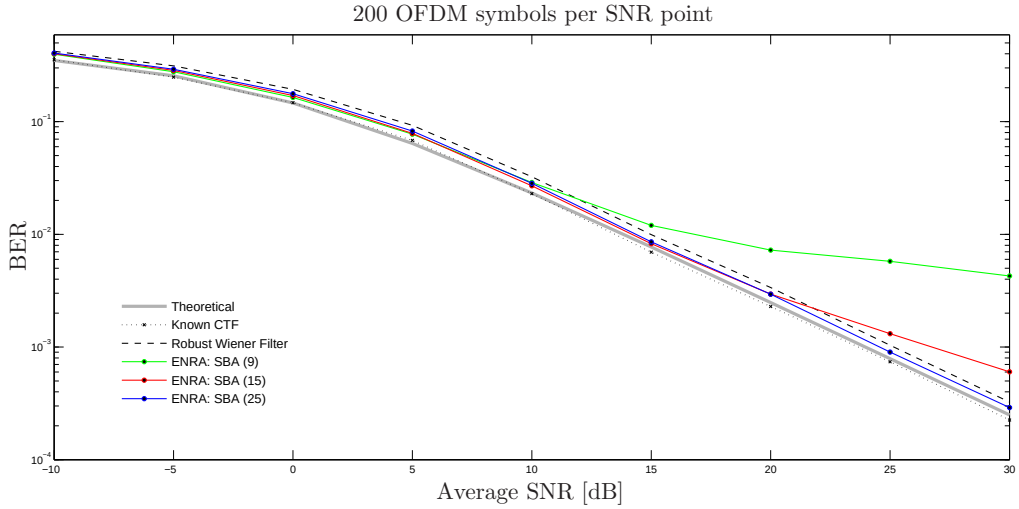

FIGURE 5.9: BER where the number of tap-delays to search for has been overestimated

three different numbers of channel echoes: 9, 15 and 25. The plot pointed out how the performance of the algorithm improve notably for high values of SNR. On the other hand it show that overestimating the number of delays the performance in the whole SNR scale tend to the RWF curve.

5.4 Chapter Summary

The SBA is investigated in this chapter in order to improve the performance keeping low the computational load. In the first section the structure of the simulator and the channel employed for run simulations are showed. Afterward, acting on the sampling grid search, some improvement are proposed and investigated in order to lower the computational complexity. The left/right search seems to be the best compromise between computational complexity and accuracy. Afterward, using this configuration we run some simulations overestimating the number of delays. The results show that collecting

25 channel echoes and using the left/right approximation we are able to outperform the RWF in the whole SNR scale.

Chapter 6

Conclusions and Future Work

The aim of this work is the multipath delays estimation using Beamforming techniques. In this work it has been showed how the RWF can be outperformed by an alternative channel estimator, the ENRA. The algorithm ENRA needs the knowledge of the channel propagation delays. These are estimated with the SBA. Initially, we evaluate SBA performance in terms of BER and MSE, pointing out how the performance improves with increased resolution in the delay domain. Furthermore, it has been observed that there is a lower bound in the resolution over that the performance does not improve anymore. A simulation study on channels with different multipath delay profiles may provide a different lower bound. However, due to time constraints, only the LTE EVA channel has been considered in this work. A notably performance degradation is observed even if just a single delay is missed in the estimation procedure. This effect is more evident for high SNR, when the echoes with too small amplitude are not detected because still masked by noise. In fact overestimating the number of delays, we obtain considerable improvement in the BER, especially for high values of SNR. On the other hand the overestimation of the number of channel echoes increases the complexity and a small performance degradation, in low SNR, is observed. We can conclude that the SBA is able to estimate the multipath delays in a nLoS Rayleigh fading channel.

6.1 Future Work

The sequential beamforming seems to be a promising delay estimation tool. Nevertheless it can still be improved both regarding performance and computational complexity. In this work it has been implemented in a static channel, but in order to have a more realistic simulations it could be interesting investigate its behavior in a dynamic channel.

The number of delays has been assumed known, but in the iterative procedure performed by the SBA it may be possible to define a stopping criteria. More than one delay may be detected at each iteration in particular when the delays are not really close. Furthermore a variety of refinements may be applied in order to improve the tap-delays resolution (for instance distinguishing main lobes from side lobes in the power spectrum) and how to remove detected peaks.

Appendix A

LTE System Setup

In the following it is explained how the pilot symbols are transmitted through the 3GPP setup proposed for LTE

A.1 Unused subchannels

Although in chapter 2, the OFDM system is designed with a total of N subchannels, in LTE not all subcarriers are used. The bandwidth used by the active carriers is called *Transmission bandwidth*:

$$B_t = N_u \Delta f$$

where N_u is the number of active subcarriers and $\Delta f = \frac{1}{T_s}$ the subcarriers spacing. The bandwidth assigned for the entire system is called *Channel bandwidth*:

$$B_c = N \Delta f$$

As shown in Figure A.1 a number of subchannels are shut down at both edges of channel

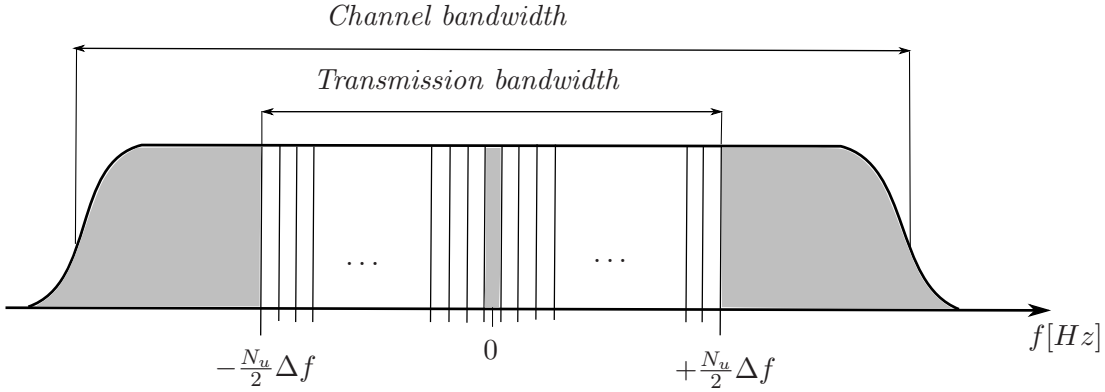

FIGURE A.1: Placement of the subcarriers in LTE setup

bandwidth. That is due to the non-existance of a filter whose frequency response is a perfect rectangular window. So to avoid the cut off of the border subchannels they are just turned off. The subchannel with frequency equal to zero is always kept inactive for technical issues [15]. The subcarriers are distributed from $-\frac{N_u}{2}$ to $\frac{N_u}{2}$, with spacing of Δf. Then, recalling the equation (2.5) and changing the summation indices, the IDFT can be written as

$$\widetilde{x}(m) = \frac{1}{\sqrt{N}} \sum_{k=-\frac{N_u}{2}}^{\frac{N_u}{2}-1} x(k+\frac{N}{2}) e^{j2\pi \frac{km}{N}} \qquad 0 \leq m \leq N-1$$

where $x(k+\frac{N}{2})$ is $x(k)$ shifted $\frac{N}{2}$ to left. If a variable change $i = k + \frac{N}{2}$ is made,

$$\widetilde{x}(m) = \frac{1}{\sqrt{N}} \sum_{i=0}^{N-1} e^{j2\pi \frac{im}{N}} e^{-j\pi m}$$

that is the IDFT of $x(k)$ (not shifted) multiplied by a phase rotation term $e^{-j\pi m}$ that simply alternate between 1 and -1. It can be implemented changing the sign on each second sample. The N-point DFT can be applied considering the following matrix

$$F = \frac{1}{\sqrt{N}} \begin{bmatrix} 1 & \omega^{-N/2} & \omega^{-2N/2} & \dots & \omega^{-(N-1)N/2} \\ \vdots & \vdots & \vdots & & \vdots \\ 1 & \omega^{-1} & \omega^{-2} & \dots & \omega^{-(N-1)} \\ 1 & 1 & 1 & \dots & 1 \\ 1 & \omega^{1} & \omega^{2} & \dots & \omega^{(N-1)} \\ \vdots & \vdots & \vdots & & \vdots \\ 1 & \omega^{N/2-1} & \omega^{2(N/2-1)} & \dots & \omega^{(N-1)(N/2-1)} \end{bmatrix} \tag{A.1}$$

that is merely a shifted version of the matrix introduced in (2.7).
In order to give an idea about the dimension of a real system, a set of parameters for downlink OFDM in LTE is shown in Table A.1

FFT size	$T_s + T_{cp}$	Δf	N_u	τ_s
2048	$71.4\mu s$	$15kHz$	1200	$32.55ns$

TABLE A.1: LTE parameters

A.2 Radio frame structure

In the time domain the consecutive transmission of OFDM symbols is organized in radio frames. In the 3GPP technical specifications, two different type of radio frame are

presented. The first one is illustrated in Figure A.2 and it is considered in this work, the second is realized for keep back-compatibility with older 3GPP standard. The duration of a radio frame is $10ms$ and it contains ten subframe. The latter consists of two slots whose duration is half a millisecond. In each slot are contained seven OFDM symbols included cyclic prefix. The cyclic prefix in the first OFDM symbol is 160 samples long, while the remaining six are 144 samples long. Then, for a LTE setup with a FFT size of 2048 the duration of each slot is

$$[160 + 2048 + 6(144 + 2048)]\tau_s \cong 0.5\ ms$$

Therefore for each frame there are $7 \times 2 \times 10 = 140$ OFDM symbols and a transfer of 14000 symbol per second is possible with the above configuration.

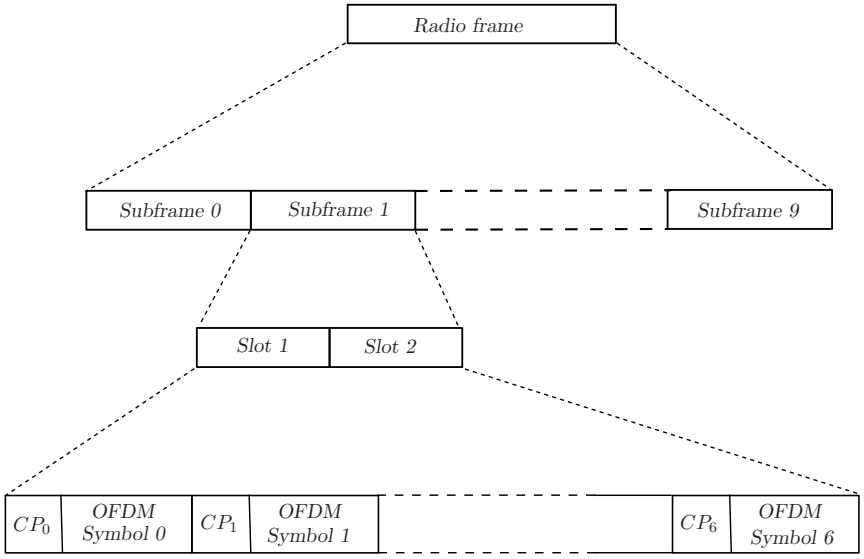

FIGURE A.2: Radio frame structure

A.3 Pilot position

The pilot assisted channel estimation is based on transmission of pilot symbol known to both transmitter and receiver. In OFDM systems, the pilot symbols are transmitted on a subset of all subcarrier, for instance $M = 200$, and they are also distributed in time domain as shown in Figure A.3. There are numerous way to distribute pilot symbol in both time and frequency domain whose configuration depends on the specific application. Of course, the use of pilot symbols introduces overhead, then it is desirable to keep the number of pilot as low as possible. Furthermore, the pilot pattern configuration depends on the multipath channel selectivity. So, if the channel is highly time variant it is useful to have pilot symbol closely spaced in time domain. Instead, if the channel is highly

frequency selective, the pilot symbol are positioned close in the frequency domain. The pilot symbol pattern suggested for LTE on the 3GPP technical specifications is shown in Figure A.3

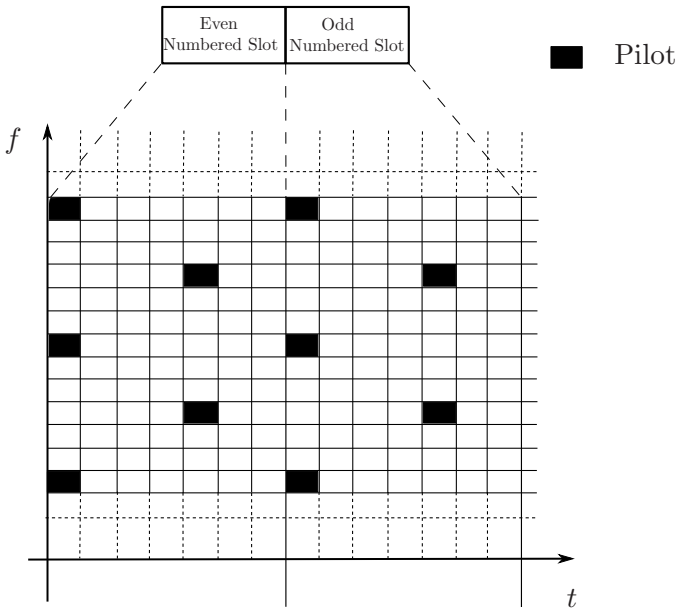

FIGURE A.3: Pilot pattern with $\gamma = 6$

Pilot symbols are distributed in both time and frequency domain. In the LTE setup they are transmitted in the first and in the fifth OFDM symbol in every slot. While in the frequency domain, the spacing between two adjacent pilots in terms of subcarriers is $\gamma = 6$. The pilot symbol pattern depicted in Figure A.3 is referred to a single transmitter. Considering a MIMO system the amount of subcarriers for data transmission is notably reduced. In Figure A.4 is shown a pilot symbol pattern in a MIMO scenario with only two transmitters. Observing carefully the pilot grid it can be seen that when the first transmitter is transmitting a pilot, the second one is not allowed to use the same time-frequency allocations in order to avoid interference. In a MIMO environment with 3 or 4 transmitter the number of subcarriers for data transmission is further reduced. Then, a minimization of pilots in this scenario, is a problem of central interest.

Being $N_u = 1200$ the number of active subcarriers and $\gamma = 6$ the spacing between two adjacent pilots in the frequency direction, the total amount of pilot within an OFDM symbol is $M = 200$. The position in the range from $-\frac{N_u}{2}$ to $\frac{N_u}{2}$ is obtained through an indexes sequence given by

$$p(m) = (\eta + \Delta i) mod 6 + (m-1)6 - \frac{N_u}{2} \qquad 1 \leq m \leq M$$

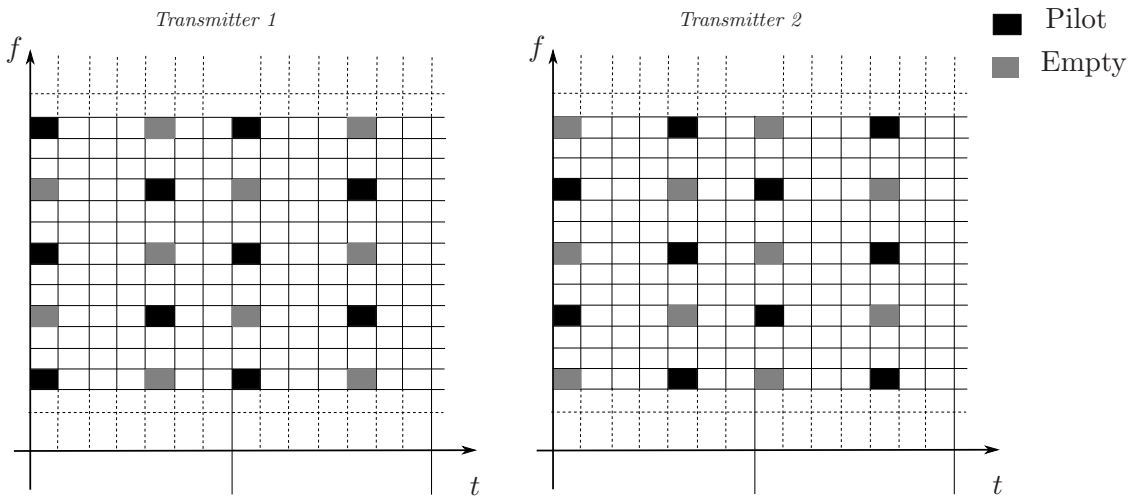

FIGURE A.4: Pilot pattern with $\gamma = 6$ and two transmitter

where $m = 1, 2, \ldots, M$ corresponds to the pilot number, Δi is the initial indent and η is given by

$$\eta = \begin{cases} 0 & \text{at the first OFDM symbol in any slot} \\ 3 & \text{at the fifth OFDM symbol in any slot} \end{cases}$$

For instance, assuming $\Delta i = 1$ an $\eta = 0$ i.e. each first OFDM symbol in every slot, the following indexes set is collected:

$$P = \{p(m)|m = 1, 2, \ldots, M\} = \{-599, -593, \ldots, -5, 2, \ldots, 590, 596\}$$

Notice that the gap between two adjacent element is always six and except where the sign changes is seven. It is due to the subchannel which central frequency is equal to zero that is shut down.

Bibliography

[1] M. L. Jakobsen. Modeling and Estimation of Wireless Multipath Channels. *Master's thesis,Aalborg University*, June 2009.

[2] Kim Laugesen. Tap-Delay Estimation for the Next-Generation of Mobile Terminals. *Master's thesis, Aalborg University*, June 2009.

[3] Andrea Goldsmith. *Wireless Communication*. 2005.

[4] 3GPP. Requirements for Evolved Universal Terrestrial Radio Access (UTRA) and Universal Terrestrial Radio Access Network (UTRAN). v 7.3.0.

[5] Farooq Khan. LTE for 4G Mobile Broadband. 2009.

[6] Jan-Jaap van de Beek, O. Edfors, M. Sandell, S.K. Wilson and P.O. Borjesson. . On Channel Estimation in OFDM Systems. *In proceedings of IEEE Vehicular Technology Conference*, 2:815–819, 1995.

[7] P. Hoeher, S. Kaiser, and P. Robertson. Two-dimensional Pilot-Symbol-Aided Channel Estimation by Wiener Filtering. *Institute for Communications Technology*, pages 1845–1848, 1997.

[8] Ove Edfors, M. Sandell, Jan-Jaap van de Beek, S.K. Wilson and P.O. Borjesson. OFDM Channel Estimation by Singular Value Decomposition. *IEEE Transactions on Communications*, 46:931–939, July 1998.

[9] Ilan Ziskind and Mati Wax. Maximum Likelihood Localization of Multiple Sources by Alternating Projection. *IEEE, Transaction on Acoustics, Speech and Signal Processing*, 36(10), October 1988.

[10] Baoguo Yang, Khaled Ben Letaief, Roger S. Cheng and Zhigang Cao. Channel Estimation for OFDM Transmission in Multipath Fading Channels Based on Parametric Channel Modeling. *IEEE Transactions on Communications*, 49:467–479, 2001.

[11] Ye (Geoffrey) Li, Leonard J. Cimini, Jr. and Nelson R. Sollenberger. Robust Channel Estimation for OFDM Systems with Rapid Dispersive Fading Channels. *IEEE Transactions on Communications*, 46:902–915, 1998.

[12] Hamid Krim and Mats Viberg. Two Decades of Array Signal Processing Research: The Parametric Approach. *IEEE Signal Processing Magazine*, 13:67–94, 1996.

[13] Vincenzo Malta. Estimation of the Number of Multipath Components in a Delay-Dispersive Environment for LTE OFDM Downlink. *Master's Thesis Aalborg University*, February 2010.

[14] Randolph Moses. Petre Stoica. Spectral Analysis of Signals. 2005.

[15] 3rd Generation Partnership Project (3GPP) Technical Specification. Evolved Universal Terrestrial Radio Access (E-UTRA); Base Station (BS) Radio Transmission and Reception . December 2008.